PAPER

Check for updates

Five and six membered heterocyclic rings endowed with azobenzene as dual EGFR^{T790M} and VEGFR-2 inhibitors: design, synthesis, *in silico* ADMET profile, molecular docking, dynamic simulation and anticancer evaluations†

Kurls E. Anwer,[a] Sanadelaslam S. A. El-Hddad, [ID] [b] Nour E. A. Abd El-Sattar, [ID] [ac] Ahmed El-morsy,[d] Fathalla Khedr,[e] Samy Mohamady,[f] Doaa E. Keshek,[gh] Samir A. Salama,[i] Khaled El-Adl [ID] *[ej] and Noura S. Hanafy[j]

Novel azobenzene scaffold-joined heterocyclic isoxazole, pyrazole, triazole, and/or triazine moieties have been developed and synthesized utilizing microwave and traditional methods. Our compounds were tested for growth inhibition of A549, MCF-7, HCT-116, and HepG2 tumors by dual targeting the VEGFR-2 and EGFR^{T790M} enzymes. The suggested compound's manner of binding with EGFR^{T790M} and VEGFR-2 active sites was explored through molecular design and MD modeling. The information from the results of the biological screening and the docking studies was highly correlated. The A549 cell line was the one that responded to the novel compound's effects most effectively. Having IC$_{50}$ values of 5.15, 6.37, 8.44 and 6.23 μM, respectively, **14** was the most effective derivative on the four A549, MCF-7, HCT116 and HepG2 cancer cells. It had greater activity than erlotinib and slightly inferior activities on the tested cell lines than sorafenib, respectively. The cytotoxicity of the most effective derivatives, **5**, **6**, **10** and **14**, was evaluated against typical VERO cell lines. Having IC$_{50}$ values ranging from 42.32 to 55.20 μM, the results showed that the investigated drugs have modest toxicity against VERO normal cells. Additionally all derivatives were assessed for their dual VEGFR-2 and EGFR^{T790M} inhibitory effects. Among them, derivatives **14**, **5** and **10** were established as the greatest inhibitors of VEGFR-2 at IC$_{50}$ values of 0.95, 1.25 and 1.50 μM correspondingly. As well, derivatives **14**, **6**, **5** and **10** could inhibit EGFR^{T790M} activity demonstrating strongest effects with IC$_{50}$ = 0.25, 0.35, 0.40 and 0.50 μM respectively. Furthermore, the ADMET profile was evaluated for compounds **5**, **6**, **10** and **14** in contrast to reference drugs sorafenib and erlotinib.

1   Introduction

A rational drug design tool for drug candidates could be achieved by molecular hybridization, which includes combination of two or more pharmacophoric groups or chemical units by either linking or fusing with each other to form new hybrid molecules, and their choice is based on their recognized bio--profiles in the hope that this hybridization could produce compounds with more powerful pharmacological activities. This strategy is often used since some of these hybrid

[a]*Department of Chemistry, Faculty of Science, Ain Shams University, Abbassia, Cairo, Egypt*

[b]*Pharmaceutical Chemistry Department, Faculty of Pharmacy, Omar Almukhtar University, Libya*

[c]*Basic & Medical Sciences Department, Faculty of Dentistry, Alryada University for Science & Technology, Egypt*

[d]*Pharmaceutical Chemistry Department, College of Pharmacy, The Islamic University, Najaf, Iraq*

[e]*Pharmaceutical Medicinal Chemistry and Drug Design Department, Faculty of Pharmacy (Boys), Al-Azhar University, Nasr City 11884, Cairo, Egypt. E-mail: khaled.eladl@hu.edu.eg; eladlkhaled74@azhar.edu.eg; eladlkhaled74@yahoo.com*

[f]*Pharmaceutical Chemistry Department, Faculty of Pharmacy, The British University in Egypt, Cairo, Egypt*

[g]*Department of Biology, Jumum College University, Umm Al-Qura University, P.O. Box 7388, Makkah 21955, Sudia Arabia*

[h]*Agriculture Genetic Engineering Research Institute (AGERI), Agriculture Research Centre, Giza, Egypt*

[i]*Division of Biochemistry, Department of Pharmacology, College of Pharmacy, Taif University, P.O. Box 11099, Taif 21944, Kingdom of Saudi Arabia*

[j]*Pharmaceutical Chemistry Department, Faculty of Pharmacy, Heliopolis University for Sustainable Development, Cairo, Egypt*

† Electronic supplementary information (ESI) available. See DOI: https://doi.org/10.1039/d3ra06614b

derivatives showed enhanced efficacy and had a safer toxicity profile than their parent drug candidates.[1,2]

Nitrogenous-heterocyclic rings are one of the utmost momentous groups in medicinal chemistry, and have lately been shown to introduce remarkably complicated biological characteristics. Due to their ability to mimic and interact with many biological components and produce amazing pharmacological effects, they serve as a fundamental scaffold in many drugs.[3,4]

As anticancer drugs that target EGFR-TK, several isoxazole derivatives have been identified.[5] Additionally, a variety of pyrazole compounds have been implicated in the prevention of cancer as dual EGFR and VEGFR-2 TK inhibitors.[6] Triazole derivatives are being utilized to treat various kinds of illnesses, including cancer.[4,7] There are many anticancer medications with the 1,2,4-triazole ring on the market, including vorozole, letrozole and anastrozole (Fig. 1).[4] Additionally, the triazine scaffold serves as a fundamental framework for the syntheses of several bioactive molecules with wide-ranging medical applications.[1,2] Numerous studies examined the progress that had been made in the triazine candidates that acted via various protein kinases inhibition, including tubulin polymerization, EGFR (EGFR^{WT} and EGFR^{T790M}), hDHFR, human topoisomerase IIα, carbonic anhydrase (CA), PI3Kα/mTOR, and CDK2, to have highly promising antitumor activity.[8,9] FDA-approved triazine-containing anticancer medications include tretamine, gedatolisib, KY-04031, altretamine, enasidenib, and HL 010183 (Fig. 1).[4]

Azobenzenes, contain N=N linkages, are endowed with diversity of uses as antituberculotic, antitumor, antiviral,

antidiabetic, anti-inflammatory, and antimicrobial agents.[10] The potential of azobenzene to act as a trigger in several biomedical fields exhibited a thorough review.[11,12] Azobenzene photo-switch can be utilized in protein structure and function photo-control, as well as kinases, proteases,[13] ion channels,[14] and G-coupled-protein receptor.[15] Particularly, azobenzene has been integrated with PROTACs for target proteins photo-controlled degradation.[16] Azobenzene is also frequently employed to accurately manipulate lipid membranes biophysics (e.g. permeability and fluidity).[17] Azobenzenes have also been used to regulate nucleic acids for enzymatic reactions and gene expression photo-regulation.[18] Moreover, different derivatives containing azobenzene moieties were reported as VEGFR-2 inhibitors.[19]

EGFR and VEGFR-2 are bounded in different disorders pathogenesis and different sets of carcinoma growth. Both have strong correlations and split common lower down signaling routes. The inter-correlations amidst VEGFR-2 and EGFR has been well-recognized: inhibition of signaling pathway of VEGFR-2 enhances the anticancer activity of EGFR inhibitors, whilst stimulating VEGFR-2 is independent on EGFR signaling which obstructs the EGFR inhibitors.[20] Therefore, blocking both signaling pathways of VEGFR and EGFR synchronously appears to be an excellent strategy in treatment of cancer.[21–23]

1.1 Structure-based and rationale design

The rational design of the target compounds kept inhibitors of both EGFR and VEGFR-2 in the essential pharmacophoric form.
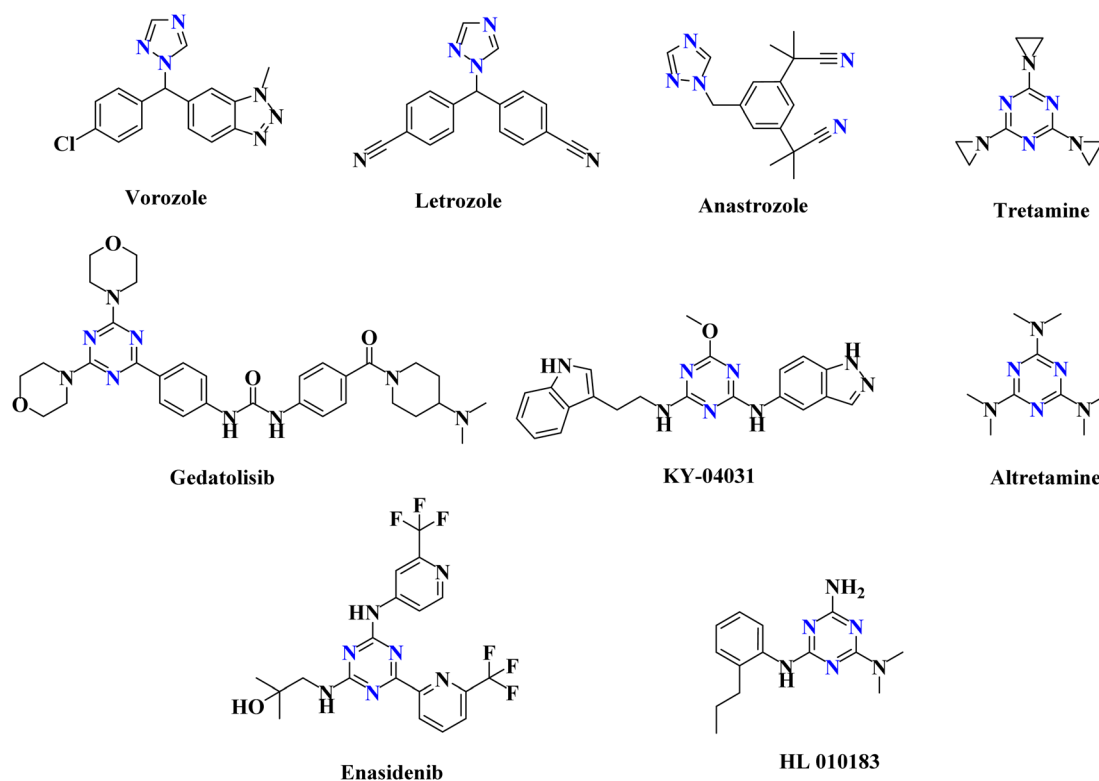

Fig. 1 FDA-approved anticancer medications with 1,2,4-triazole and triazine rings.

A novel series of azobenzene endowed with heterocyclic moieties were designed and synthesized according to the essential VEGFR-2 inhibitors pharmacophoric structures as a continuation of our efforts to discover new agents for anti-cancer treatment.[24–40] Four key characteristics were found to be shared by sorafenib and different VEGFR-2 inhibitors (Fig. 2);[41–43] the terminal hydrophobic part which occupy the allosteric hydrophobic fissure forming hydrophobic bonds, pharmacophore linker with amino or urea functional groups that bind to the essential amino acids Glu883 and Asp1044, central hydrophobic spacer and a flat hetero aromatic ring system.

Our molecular design synthetic strategy focused on bio-isosteric modification of sorafenib & pazopanib as inhibitors of VEGFR-2 at the different four parts (Fig. 2).

However, our novel compounds also displayed the EGFR-TKIs pharmacophoric structures, such as: (i) a lipophilic head that resides in the hydrophobic area. (ii) The adenine adherence pocket forms an interaction with a hetero aromatic ring. (iii) H-bond donor/and or acceptor[42] *e.g.* NH group, which might interact at the linker domain with an amino acid to create strong hydrogen bonds. (iv) A hydrophobic tail that connects to the hydrophobic region II,[44,45] (Fig. 3). Our investigation into SAR of synthetic anti-cancer compounds with combined EGFR[T790M] and VEGFR-2 preventive events was inspired by all of these alterations.

2 Results and discussion

2.1 Chemistry

Syntheses of new isoxazolone, pyrazalone, 1,2,4-triazole and 1,2,4-triazine derivatives following the reactions described in (Schemes 1–3). The starting material ethyl 2-cyano-2-{[4-(phenyldiazenyl)phenyl]-diazenyl}acetate (2) was synthesized *via* treatment of 4-aminoazobenzene with $NaNO_2$ and HCl at 0–5 °C giving the corresponding diazonium chloride 1 which undergo coupling with ethyl cyanoacetate to produce the starting material 2 (Scheme 1). Compound 2 IR spectrum
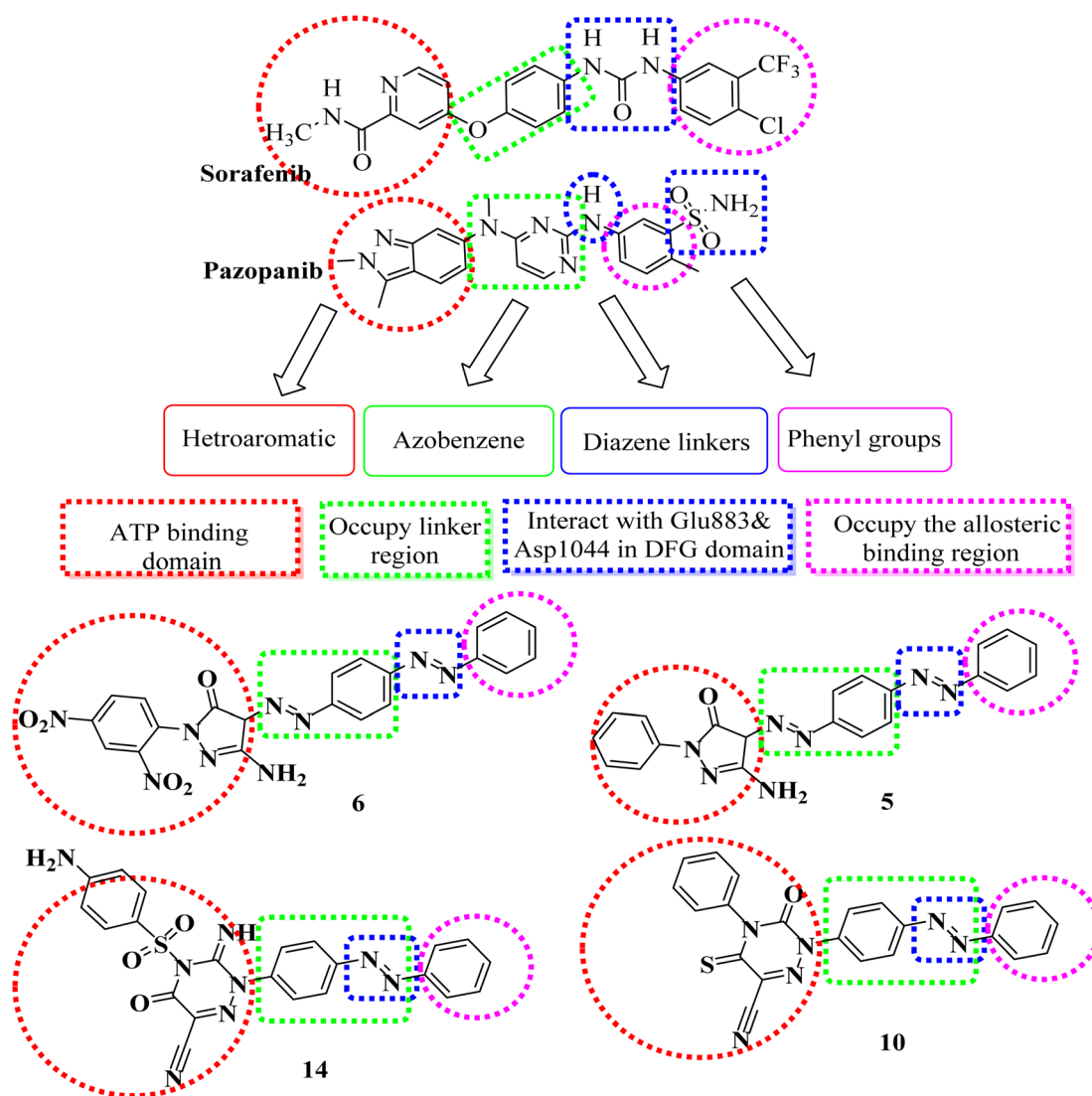

Fig. 2 Pharmacophoric and structural similarities of some designed compounds and VEGFR-2 inhibitors.
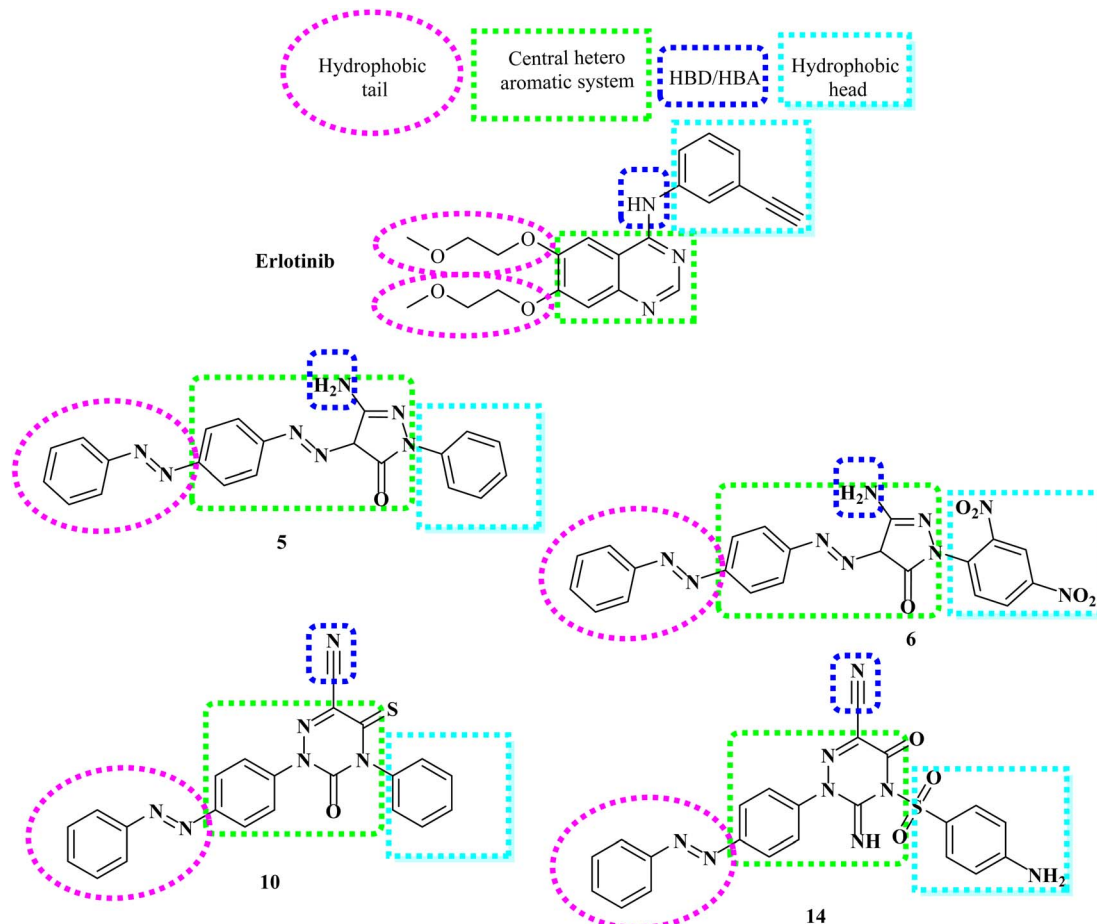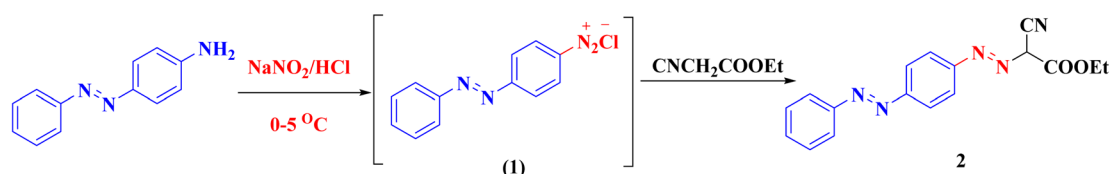
Fig. 3 Design rationale based on structural characteristics of EGFR inhibitors.

Scheme 1 Synthesis of compound **2**.

illustrated characteristic bands for $C\equiv N$ at 2225, $C=O$ at 1741, and 2 $N=N$ at 1489 and 1470. Also, the ^{1}H-NMR and ^{13}C-NMR spectra of compound **2** were consistent with the formed structure.
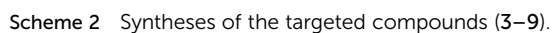
Compound **2** was cyclized with hydroxylamine hydrochloride in the existence of anhydrous K_2CO_3 to give the targeted isoxazolone **3**. This reaction proceeds *via* the nucleophilic attack of NH_2 on cyano group then nucleophilic addition of OH group on $C=O$ group followed by elimination of one molecule of ethanol. The structure of **3** showed IR absorption bands at 3461, 3346 (NH_2), 3190 (NH), 1686 cm^{-1} ($C=O$). Compound **3** proton NMR showed 7.51–7.93 (m, 9H, Ar-H), 8.60 (s, 2H, NH_2, D_2O exchangeable), and 15.95 (s, 1H, NH, D_2O exchangeable).

Also, compound **2** underwent cyclization with hydrazine hydrate, phenyl hydrazine, 2,4-dinitrophenyl hydrazine (DNP)

and semicarbazide hydrochloride to obtain the corresponding pyrazolone derivatives **4–7**, respectively. The proposed structures of **4–7** were confirmed by the disappearance of cyano bands and ester carbonyl bands but presence of NH_2, NH and pyrazolone carbonyl bands, in their IR spectra.

Alternatively, cyclization of compound **2** with thiosemicarbazide was interestingly proceeds in another manner to produce 1,2,4-triazole derivative **9** instead of the expected pyrazolone derivative **8** (ESI†). Analytical and spectroscopic examinations of **9** led to the characterization of its chemical composition and structure. For instance, the compound's IR spectra showed $C\equiv N$ band at 2226 cm^{-1}, but no NH_2 or $C=O$ bands. The proton NMR of **9** disclosed a signal at 4.49, 7.19 and 8.62 ppm specific for the 3NH groups as well as its ^{13}C-NMR revealed a singlet signal at 181.6 ppm specific for $C=S$ group (Scheme 2).
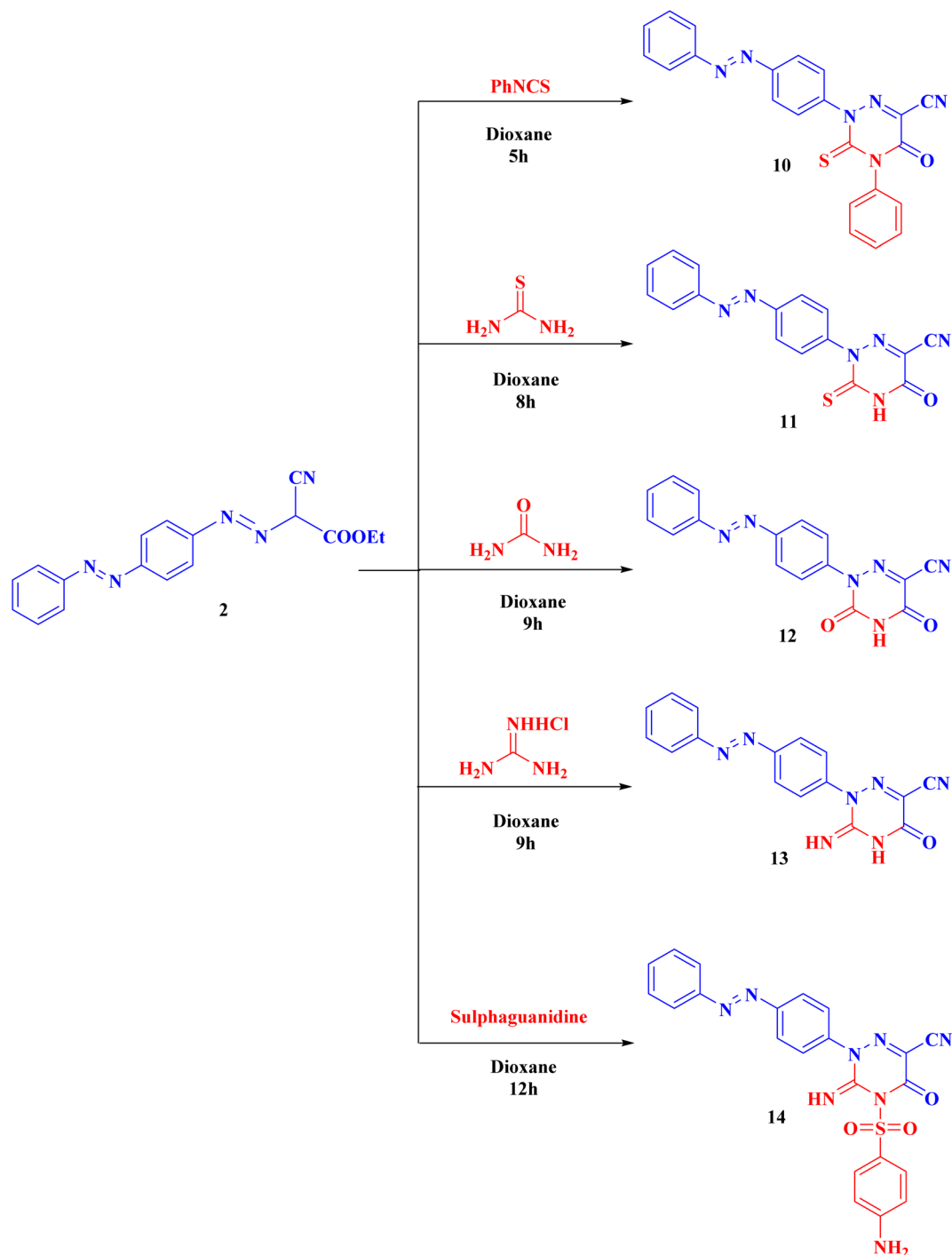
Scheme 2 Syntheses of the targeted compounds (**3–9**).

Compound **2** can be used as a fundamental intermediate for the syntheses of new 1,2,4-triazine derivatives *via* its cyclization reactions with phenyl isothiocyanate, thiourea, urea, guanidine hydrochloride, and/or sulphaguanidine to form compounds **10–14**, respectively. Compound **10** was cyclized by nucleophilic attack of the NH group on the C=S of the isothiocyanate group followed by intramolecular cyclization with removal of one ethanol molecule. Compounds **11–14** were obtained (Scheme 3) through the nucleophilic attack on the ester carbonyl by the NH group followed by loss of one ethanol molecule, then intramolecular rearrangement with elimination of one molecule of ammonia leading to ring cyclization *via* nucleophilic addition (ESI†).

Our compounds were produced utilising microwave technology and conventional methods[46–50] (ESI†).

2.2 Docking studies

Molsoft program was used in this modeling research. Both EGFR^{T790M} (PDB ID 3W2O)[45] and VEGFR-2 (PDB ID 4ASD)[51] were subjected to manipulation in each experiment.

2.2.1 As VEGFR-2 inhibitors. In the active site of VEGFR-2, all ligands are positioned and oriented similarly (ESI†). According to the binding energy (ΔG), the mainstream of these drugs demonstrated very good VEGFR-2 affinity (Table 1).

Scheme 3 Syntheses of the targeted derivatives (**10**–**14**).

Five H-bonds and −99.50 kcal mol^{-1} were found for sorafenib. It made one H-bond with Asp1046 (1.50 Å), 2 hydrogen bonds with Glu885 (2.75 Å and 1.77 Å) and 2 hydrogen bonding interfaces with *Cys919* (2.51 Å and 2.10 Å). The hydrophobic groove created by *Leu1035*, *Cys1045*, *Val848* and *Lys868* is wrapped by the central phenyl linker. Additionally, the hydrophobic channel formed by *Ile892*, *Ile888*, *Hie1026*, *Glu885*, *Cys1045*, and *Asp1046* was dominated by the distal 3-trifluromethyl-4-chlorophenyl array. In excess, *N*-

methylpicolinamide set assimilated inside the cleft constructed by *Cys919*, *Phe918*, *Glu917*, *Lys920*, *Val848*, *Leu1035* and *Leu840* (Fig. 4).

Compound **14** exhibited −102.62 kcal mol^{-1} and 5 hydrogen bonds. The SO$_2$ group exhibited two hydrogen bonds with *Cys919* (2.45 Å and 2.79 Å). The NH$_2$ group showed one H-bond with *Leu840* (2.73 Å). Moreover, the cyano group displayed one H-bond with Ile849 (2.19 Å). Also the diazene linker displayed one hydrogen bond with *Asp1046* (1.87 Å). The socket created by

Table 1 ΔG in kcal mol^{-1} for VEGFR-2 binding ligands

Compound	ΔG [kcal mol^{-1}]	Compound	ΔG [kcal mol^{-1}]
3	−85.25	10	−91.59
4	−93.97	11	−77.72
5	−99.64	12	−78.46
6	−98.92	13	−82.37
7	−85.71	14	−102.62
9	−85.89	Sorafenib	−99.50

Lys868, *Leu1035*, *Val848*, *Ile849*, *Leu840*, *Ly920*, *Phe918*, *Cys919*, and *Glu917* was filled by the heterocyclic *p*-aminophenylsulfonyltriazine molecule. As well, the hydrophobic groove shaped by *Leu1035*, *Lys868*, *Glu917*, *Cys1045* and *Asp1046* has an azobenzene spacer built into it. The hydrophobic vessel generated by *Cys1045*, *Ile892*, *Asp1046*, *Hie1026*, *Ile888*, *Glu885*, *Ile1044* and *Glu885* was likewise filled by the terminal benzene ring (Fig. 5).

Compounds 5 showed nearly the same binding mode of 14 with −78.04 kcal mol^{-1} and 4 H-bonds. It formed one H-bond with *Cys919* (2.47 Å), two hydrogen bonds with *Glu917* (1.68 Å and 1.69 Å) and one H-bond with *Asp1046* (1.68 Å). 5-Amino-2-phenylpyrazol-3-one occupies the hollow formed *via* *Lys868*, *Val848*, *Leu1035*, *Ile849*, *Cys919*, *Phe918*, *Lys920*, *Leu840* and *Glu917*. While compound 10 exhibited −76.05 kcal mol^{-1} and 4 H-bonds. It linked to *Cys919* through two H-bonds (1.68 Å and 2.99 Å), one hydrogen bond with *Glu917* (2.79 Å) and one H-bond with *Asp1046* (2.07 Å). The heterocyclic 5-oxo-4-phenyl-3-thioxo-1,2,4-triazine-6-carbonitrile occupies the channel formed *via* *Lys868*, *Val848*, *Leu1035*, *Ile849*, *Cys919*, *Phe918*, *Lys920*, *Leu840* and *Glu917* (ESI†).

2.2.2 As EGFR^{T790M} inhibitors. The deduced corollaries displayed that all investigated derivatives had the same locations and orientations inside the known EGFR binding region (ESI†). According to binding energy (ΔG), most of these congeners exhibited very good EGFR binding affinities (Table 2).

Four H-bondings and −82.77 kcal mol^{-1} were seen with Erlotinib. The quinazoline scaffold is linked to *Valine726* and *Methionine793* through one H binding each with 2.97 Å and 1.82 Å respectively. One 2-methoxyethoxy moiety is linked to *Cys797* through one H binding (2.05 Å). Also NH spacer is linked to *Thr854* through H-bond (2.99 Å). The hydrophobic domain I created with *Ile759*, *Phe723*, *Gly724*, *Val726*, *Glu762*, *Leu777*, *Thr854*, *Glu791*, *Met790*, and *Asp855* was linked to the 3-ethynylphenyl head. In addition, the 2-methoxyethoxy end made hydrophobic interactions with the groove II that was created by *Val 845*, *Met 793*, *Leu 718*, *Pro 794*, and *Leu 844* (Fig. 6).

Compound 14 exhibited 6 H-bonds and −87.16 kcal mol^{-1}. The NH$_2$ group linked with *Glu762* through two H-bonds (1.71 Å and 2.60 Å). Also SO$_2$ exhibited two hydrogen bonds with *Gly724* (2.56 Å and 2.67 Å). Additionally, the cyano group linked with *Lys754* through H-bond (2.77 Å). Furthermore the triazine ring linked with *Thr854* through hydrogen bond (2.99 Å). The azobenzene end occupies the hydrophobic region II built *via* *Pro794*, *Met793*, *Leu718*, *Val726*, *Val845*, *Cys797* and *Leu844*. Moreover, the 5-amino-2-phenylpyrazol-3-one head occupies the hydrophobic zone I created by *Leu788*, *Glu762*, *Ile759*, *Gly724*, *Phe723* and *Asp855* (Fig. 7).

Structure 6 is approximately the same as 14 with 4H-bonds and −82.90 kcal mol^{-1}. It made 4 hydrogen bonds with *Asp855* (2.36 Å), *Thr854* (1.75 Å and 2.98 Å), and *Lys745* (2.14 Å). The azobenzene end occupies the hydrophobic region II built *via* *Pro794*, *Met793*, *Leu718*, *Val726*, *Cys797* and *Leu844*. Moreover, 5-amino-2-(2,4-dinitrophenyl)pyrazol-3-one head filled the
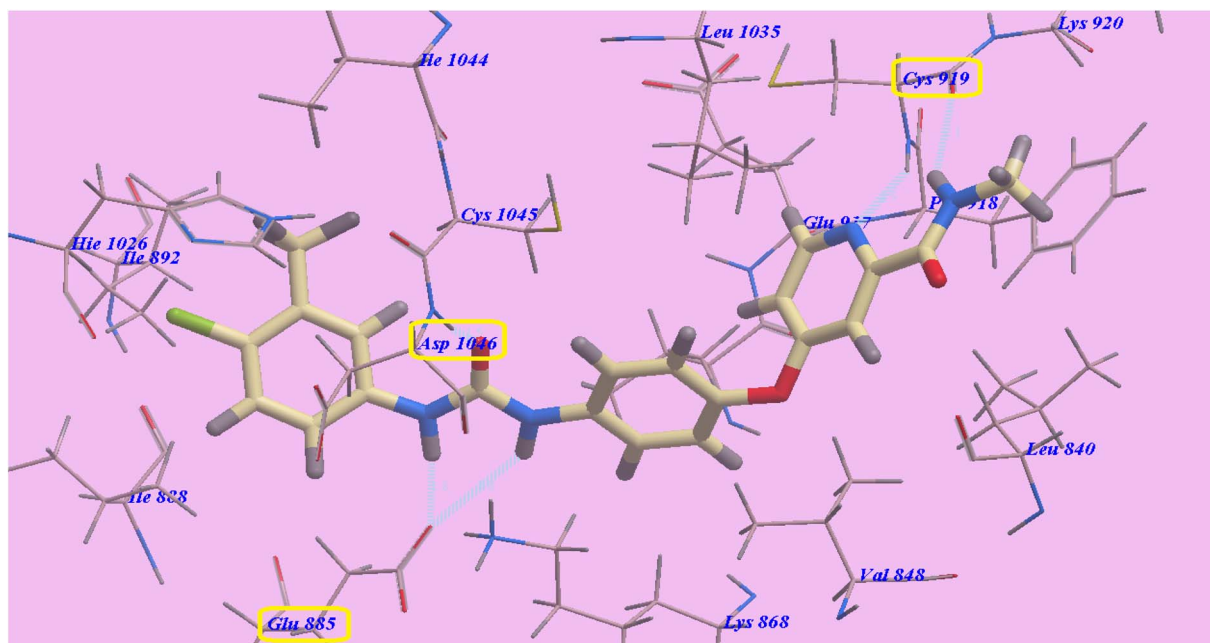
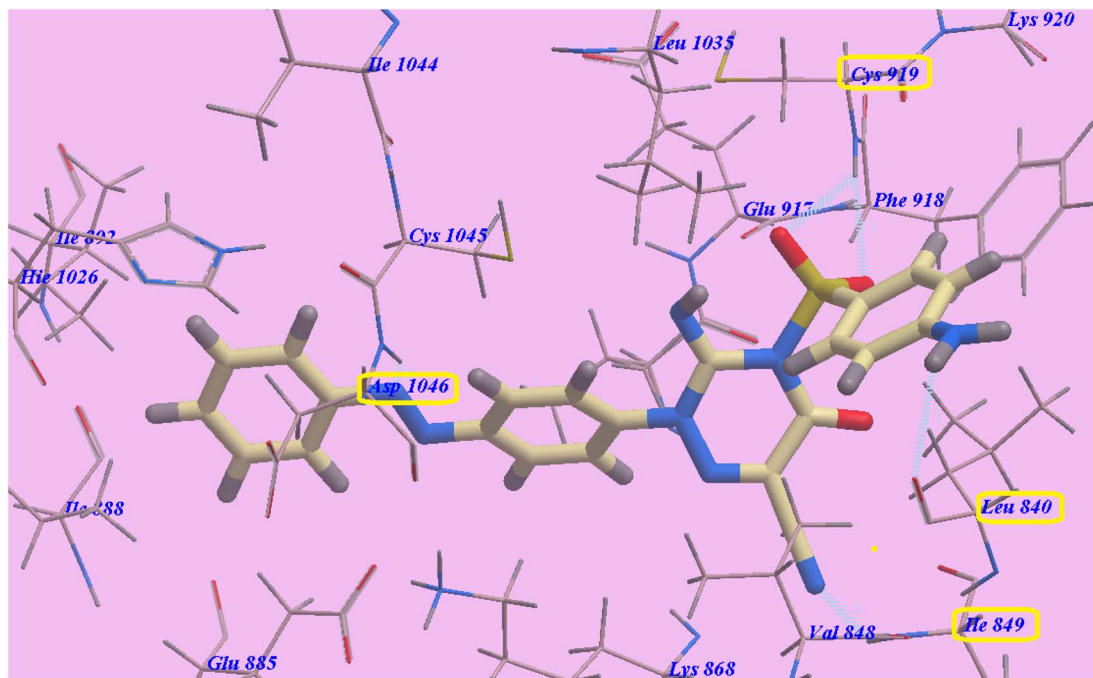

Fig. 4 Predicted 4ASD binding mechanism of sorafenib.

Fig. 5 Compound **14**'s predicted binding mode with 4ASD.

Table 2 Ligands ΔG (kcal mol^{-1}) for binding with EGFR^{T790M}

Compound	ΔG [kcal mol^{-1}]	Compound	ΔG [kcal mol^{-1}]
3	−63.49	**10**	−76.05
4	−66.21	**11**	−60.33
5	−78.04	**12**	−67.58
6	−82.90	**13**	−65.36
7	−71.84	**14**	−87.16
9	−66.15	Erlotinib	−82.77

hydrophobic zone I created by *Leu788*, *Glu762*, *Ile759*, *Gly724*, *Phe723* and *Asp855*. Also derivative **5** showed three H-bonding interactions and −78.04 kcal mol^{-1}. It made 3 hydrogen bonds with *Asp855* (2.47 Å) and *Thr854* (2.06 Å and 2.97 Å) (ESI†).

2.3 Molecular dynamics simulation

The highly active derivatives **5**, **6**, **10** and **14** in the proteins VEGFR-2 and EGFR^{T790M} were simulated using molecular dynamics (MD). By utilizing Amber's MM/GBSA.py script and the trajectory, the receptor-ligand binding energy was calculated.[52] Additionally, the employed as positive controls were sorafenib and erlotinib. With the help of GAFF2 (ref. 53 and 54) and the force field AMBERff14SB for the protein, ligand force fields were produced.[55] The monitored root mean square deviation (RMSD) validated the studied inhibitor compound's considerable global stability inside the target's recognized active site throughout the 30 ns all-atom MD runs (Fig. 8). A given ligand's molecular divergence from a defined original/ reference structure is estimated using RMSD. The selected

MD simulation procedure was valid, and it gave a respectable suggestion of the stability of the ligand-target interaction.

2.4 Biological testing

2.4.1 *In vitro* cytotoxic effects. Anti-proliferative effects of the novel derivatives **3–14** was tested on four cell lines, A549, MCF-7, HCT-116, and HepG2 using MTT assay.[56–58] The reference drugs sorafenib and erlotinib were used in the experiments. Table 3 showed the resulted values of IC$_{50}$ for our derivatives. A549 was the greatest affected cell line by our derivatives correspondingly. Compound **14** was the utmost effective derivative on the four A549, MCF-7, HCT116 and HepG2 cancers with IC$_{50}$ = 5.15, 6.37, 8.44 and 6.23 μM respectively. It presented slightly lower activities than sorafenib, (IC$_{50}$ = 4.00, 5.05, 5.58 and 4.04 μM respectively), and revealed higher activities than erlotinib (IC$_{50}$ = 7.73, 13.91, 8.20 and 5.49 μM respectively) against the four cell lines.

With reverence to the HepG2 cell lines, derivatives **5**, **6** and **10** demonstrated very high anticancer effects with IC$_{50}$ = 7.80, 8.17 and 6.81 μM respectively. Compounds **3**, **4**, **7** and **9**, with IC$_{50}$ ranging from 10.55 to 19.00 μM, presented good cytotoxicity. Furthermore, derivatives **12** and **13**, with IC$_{50}$ = 21.10 and 20.50 μM respectively, showed moderate cytotoxicity. Additionally, derivative **11** with IC$_{50}$ = 35.64 μM, demonstrated the lowest cytotoxicity.

Assessment of cytotoxicity on HCT-116 cell lines revealed that derivatives **5** and **10** demonstrated very high anticancer effects with IC$_{50}$ = 8.12 and 9.23 μM respectively. Compounds **3**, **4**, **6**, **7** and **9**, with IC$_{50}$ ranging from 10.10 to 17.50 μM, presented good cytotoxicity. Furthermore, compounds **12** and **13**, with IC$_{50}$ = 22.50 and 20.05 μM respectively, showed moderate
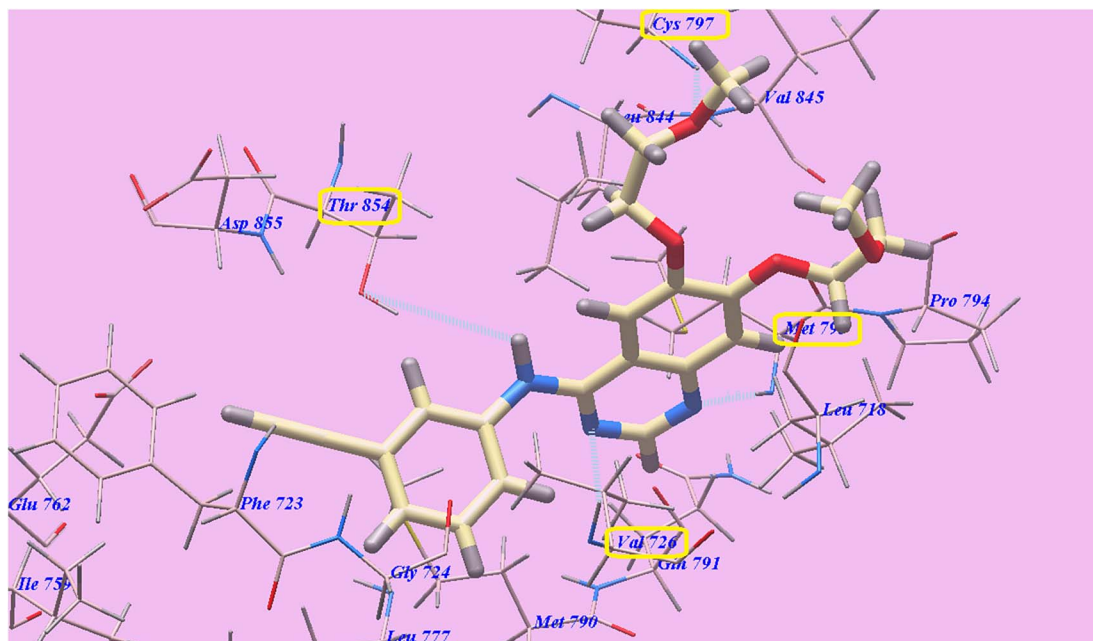
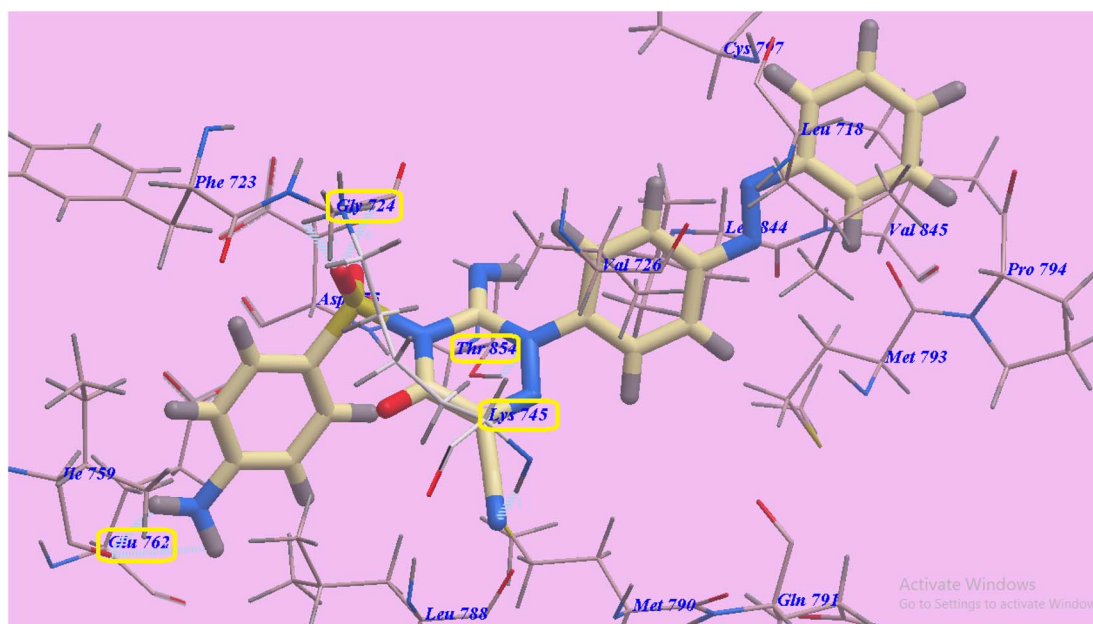Fig. 6   Erlotinib's anticipated binding style with 3W2O.

Fig. 7   Anticipated binding style for **14** with 3W2O.

cytotoxicity. Additionally, derivative **11** with IC$_{50}$ = 37.93 μM, demonstrated the lowest cytotoxicity.

Assessment of cytotoxicity on MCF-7 cell lines showed that derivatives **5**, **6** and **10** demonstrated very high anticancer effects with IC$_{50}$ = 6.98, 9.11 and 7.28 μM respectively. Compounds **3**, **4**, **7** and **9**, with IC$_{50}$ ranging from 11.33 to 17.55 μM, displayed good cytotoxicity. In addition, **13**, with IC$_{50}$ = 23.05 μM, showed moderate cytotoxicity. Finally, compounds **11** and **12** with IC$_{50}$ = 39.22 and 30.25 μM respectively, demonstrated the lowest cytotoxicity.

Assessment of cytotoxicity against A549 cell lines discovered that derivatives **5**, **6**, **7**, **10** and **12** with IC$_{50}$ ranging from 5.88 to 9.25 μM displayed very high anticancer effects. Compounds **4**, **9** and **13**, with IC$_{50}$ = 10.85, 12.25 and 15.50 μM respectively, presented good cytotoxicity. Besides, compound **3** with IC$_{50}$ = 25.50 μM, demonstrated moderate cytotoxicity. Finally, compound **11** with IC$_{50}$ = 30.25 μM correspondingly, presented the lowest cytotoxicity.

Furthermore, the greatest active compounds **5**, **6**, **10** and **14** were examined against normal VERO cell lines for their
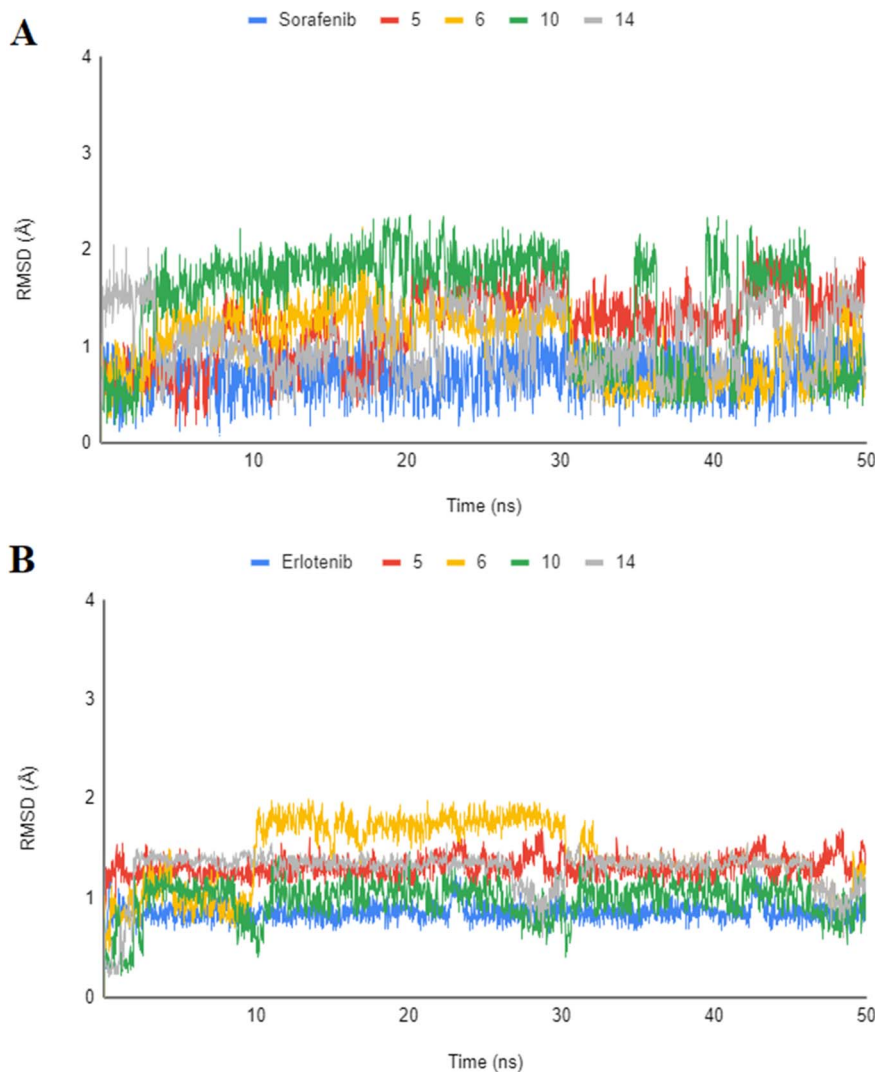
Fig. 8 Analysis of RMSD throughout 50 ns for the ligand–protein complexes all-atom MD simulation. (A) VEGFR-2 protein RMSD; (B) EGFR[T790M] protein RMSD.

Table 3 EGFR[T790M]/VEGFR-2 kinases assays and *in vitro* anticancer activities of our new derivatives against VERO cell lines, A549, MCF-7, HCT-116 and HepG2

Comp.	IC$_{50}$[a] (μM)						
	HepG2	HCT116	MCF-7	A549	VERO	VEGFR-2	EGFR[T790M]
3	19.00 ± 4.4	16.75 ± 3.7	17.55 ± 4.5	25.50 ± 3.5	NT[b]	3.25 ± 0.50	2.10 ± 0.25
4	10.55 ± 3.0	11.27 ± 3.1	11.33 ± 3.3	10.85 ± 1.5	NT[b]	1.85 ± 0.10	1.20 ± 0.35
5	7.80 ± 0.7	8.12 ± 0.9	6.98 ± 1.1	6.50 ± 1.5	44.60 ± 0.31	1.25 ± 0.50	0.40 ± 0.35
6	8.17 ± 2.6	10.10 ± 2.9	9.11 ± 2.7	5.88 ± 0.5	45.15 ± 0.43	1.60 ± 0.50	0.35 ± 0.15
7	15.60 ± 3.5	17.50 ± 4.0	14.25 ± 3.5	8.50 ± 0.5	NT[b]	2.35 ± 0.20	0.90 ± 0.25
9	14.50 ± 2.8	16.75 ± 3.3	13.80 ± 3.0	12.25 ± 2.5	NT[b]	2.00 ± 0.10	1.35 ± 0.15
10	6.81 ± 1.9	9.23 ± 2.2	7.28 ± 2.4	7.35 ± 1.5	42.32 ± 0.31	1.50 ± 0.10	0.50 ± 0.25
11	35.64 ± 4.8	37.93 ± 4.6	39.22 ± 4.8	30.25 ± 3.5	NT[b]	3.85 ± 0.50	2.50 ± 0.35
12	21.10 ± 4.9	22.50 ± 4.8	30.25 ± 4.8	9.25 ± 1.5	NT[b]	3.50 ± 0.50	0.95 ± 0.35
13	20.50 ± 4.2	20.05 ± 3.5	23.05 ± 3.8	15.50 ± 2.5	NT[b]	3.35 ± 0.50	1.50 ± 0.15
14	6.23 ± 2.3	8.44 ± 2.6	6.37 ± 2.5	5.15 ± 1.5	55.20 ± 0.32	0.95 ± 0.10	0.25 ± 0.15
Sorafenib	4.00 ± 0.33	5.05 ± 0.50	5.58 ± 0.55	4.04 ± 0.33	NT[b]	0.84 ± 0.04	NT[b]
Erlotinib	7.73 ± 0.67	13.91 ± 1.3	8.20 ± 0.34	5.49 ± 0.45	NT[b]	NT[b]	0.24 ± 0.22

[a] IC$_{50}$ values are the mean ± S.D. of three separate experiments. [b] NT = Not tested.

cytotoxicity. The results discovered that the tested derivatives with IC$_{50}$ values ranging from 42.32 to 55.20 μM showed low toxicity against VERO normal cells. Compounds **5, 6, 10** and **14** are respectively, 5.72, 5.49, 6.39 and 6.86 fold times more toxic in toxic in HepG-2 than in VERO normal cells. Uniformly, derivatives **5, 6, 10** and **14** are consequently 5.53, 4.47, 4.96 and 7.68 folds toxic in HCT-116 than in normal VERO cells. Furthermore, structures **5, 6, 10** and **14** are respectively 6.21, 4.59, 5.81 and 5.76 folds toxic in MCF-7 than in ordinary VERO cells. Furthermore, products **5, 6, 10** and **14** are respectively 8.86, 6.54, 8.67 and 10.72 folds toxic in A549 than in ordinary VERO cells.

2.4.2 VEGFR-2 kinase inhibitory assay. Additionally, using an anti-phosphotyrosine antibody with the Alpha Screen system (PerkinElmer, USA), all compounds were tested for their inhibitory effects on VEGFR-2.[59] Table 3 shows that all derivatives had good to strong inhibitory effects, with IC$_{50}$ values ranging from 0.95 to 3.85 μM. Derivatives **14, 5**, and **10** were discovered to be the greatest effective of them all, inhibiting VEGFR-2 at IC$_{50}$ values of 0.95, 1.25, and 1.50 μM, respectively. Compounds **4** and **6** demonstrated very good activity with the IC$_{50}$ = 1.85 and 1.60 μM respectively. Also, compounds **7** and **9** showed good VEGFR-2 inhibition with IC$_{50}$ = 2.35 and 2.00 μM respectively. On the other hand compounds **3, 11, 12** and **13** moderately inhibited VEGFR-2 at IC$_{50}$ ranging from 3.25 to 3.85 μM.

2.4.3 EGFR^{T790M} kinase inhibitory assay. EGFR overexpression has been linked to high violence, a poor prognosis and metastasis in a number of malignancies, including HepG2 and A549 cell lines.[60] As a consequence, using the HTRF (homogeneous time resolved fluorescence) assay, all drugs were assessed for their ability to inhibit mutant EGFR^{T790M}.[61] With an IC$_{50}$ = 0.24, erlotinib was employed as the reference. Table 3 compares the IC$_{50}$ values of the tested compounds.

Derivatives **14, 6, 5** and **10** could inhibit EGFR^{T790M} activity demonstrating strongest effects with IC$_{50}$ = 0.25, 0.35, 0.40 and

0.50 μM respectively. Derivatives **4, 7, 9, 12** and **13** considerably inhibited EGFR^{T790M} at IC$_{50}$ ranging from 0.90 to 1.50 μM. Conversely compounds **3** and **11** moderately inhibited EGFR^{T790M} at IC$_{50}$ values of 2.10 and 2.50 μM respectively.

2.4.4 Structure activity relationship (SAR). The information acquired showed that the examined structures showed varying degrees of anticancer activity and had a unique pattern of selectivity for the A549 cell lines. In general, the type of the substituent's electronic, lipophilicity nature, heterocyclic ring, the spacer and linker (HBA-HBD) all played a significant impact in their anticancer actions. Our derivatives with azobenzene spacers and diazene linkers (HB acceptors) impart high affinities towards both VEGFR-2 and EGFR^{T790M} receptors with very good anticancer activities. The triazine heterocyclic derivative **14** showed greater activity than pyrazole, triazole **9**, and oxazole **3** derivatives, respectively.

We are able to categorize the tested derivatives into two categories based on the structure of the synthesized derivatives and the data shown in Table 3. The first category consists of compounds **3–9**, which include heterocyclic rings with five members that are isoxazole, pyrazole, or triazole. Generally, the pyrazole derivatives exhibited higher activities than triazole and isoxazole derivatives respectively. The isoxazole derivative **3** exhibited the lowest activities against HepG2, A549 and MCF-7 but against HCT116 it showed anticancer activity equipotent to that of triazole derivative **9**. The tiazole **9** revealed higher activities than pyrazole **7** against the tested cell lines except A549. Against HepG2, MCF-7, and HCT116 cell lines, pyrazole derivative **5** with a more lipophilic phenyl group shown stronger activities than **6** with lipophilic electron withdrawing 2,4-dinitro substituents, less lipophilic pyrazole derivative **4** without a phenyl ring, and **7** with carboxamide, whereas against A549 the order of activity is **6 > 5 > 7 > 4**.
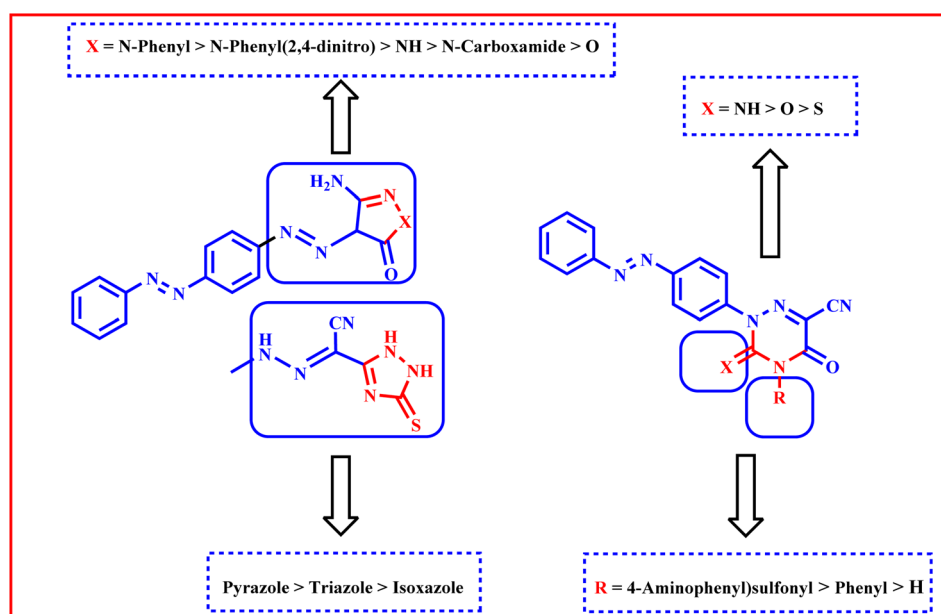

Fig. 9 Schematic presentation for SAR study.

The second group is compounds **10–14** which containing triazine heterocyclic ring; where the more lipophilic derivative **14** with electron withdrawing 4-aminophenylsulfone and 3-imino showed higher activities than **10** with lipophilic 4-phenyl and 3-thioxo, less lipophilic **13** with 3-imino and no phenyl ring, **12** with 3-oxo and no phenyl ring and **11** with 3-thioxo and no phenyl ring against HepG2, HCT116 and MCF-7 but against A549 the order is **14** > **10** > **12** > **13** > **11** (Fig. 9).

2.5 *In silico* ADMET profile

The highly active compounds **5, 6, 7, 9, 10** and **14** were subjected to *in silico* study of their proposed ADMET profile and the physicochemical characters evaluation. It was expected using pkCSM descriptor algorithm procedures[62] and corresponding to Lipinski's rule of five.[63] For the compounds that comply with at least three rules, the favorable absorption characteristics were predictable: (i) hydrogen bond donors should not exceed five, (ii) partition coefficient ($\log P$) should not exceed five, (iii) molecular weight should not exceed 500, (iv) hydrogen bond acceptors should not exceed ten. The traditional anticancer drug sorafenib and our derivatives **6, 10**, and **14** all violate one rule in the published work, however our novel molecules **5, 7, 9** and erlotinib don't.

Our compounds have good human gastrointestinal tract (GIT) absorption (84.583 to 100), which implies that they are more simply able to cross different biological membranes,[64]

Table 4 The highest effective compounds **5, 6, 7, 9, 10** and **14**, sorafenib and erlotinib; ADMET profile[a]

Parameter	5	6	7	9	10	14	Sorafenib	Erlotinib
Physicochemical properties								
Molecular weight	383.531	473.409	350.342	348.395	410.462	472.49	464.831	393.443
Log P	4.8733	4.6897	2.7474	4.22247	5.03977	2.61975	5.5497	3.4051
Acceptors	7	11	8	7	8	11	4	7
Rotatable bonds	5	7	4	5	4	5	5	10
Surface area	166.655	195.961	147.464	147.506	176.375	192.802	185.111	169.532
Donors	1	1	2	3	0	2	3	1
Absorption								
Water solubility	−5.124	−4.759	−3.805	−3.934	−6.312	−3.651	−4.822	−4.736
Caco2 permeability	0.894	−1.077	−0.412	−0.607	0.385	−0.113	0.689	1.431
GIT absorption	100	96.005	86.122	84.583	95.101	86.405	89.043	94.58
Inhibitor of *P*-glycoprotein II	+	+	−	+	+	+	+	+
Inhibitor of *P*-glycoprotein I	+	+	+	−	+	+	+	+
Substrate for *P*-glycoprotein	+	+	+	+	+	+	+	−
Skin permeability	−2.685	−2.735	−2.802	−2.775	−2.723	−2.735	−2.767	−2.741
Distribution								
CNS permeability	−1.764	−2.263	−2.424	−2.257	−1.644	−2.654	−1.655	−3.216
BBB permeability	−0.816	−1.858	−1.137	−1.59	−0.963	−1.522	−1.726	−0.745
VDss (human)	0.002	−0.171	−0.427	−0.912	−0.136	−0.814	−0.625	0.199
Metabolism								
CYP3A4 substrate	+	+	+	+	+	+	+	+
CYP2D6 substrate	−	−	−	−	−	−	−	−
Inhibition of CYP2C9	+	+	−	+	+	+	+	+
Inhibition of CYP1A2	+	−	+	+	+	−	+	+
Inhibition of CYP3A4	+	+	−	+	+	+	+	+
Inhibition of CYP2C19	+	+	−	+	+	+	−	−
Inhibition of CYP2D6	−	−	−	−	−	−	+	+
Excretion								
Renal OCT2 subst	−	−	+	−	−	−	−	−
Clearance	−0.407	−0.426	−0.309	−0.011	−0.152	0.103	−0.219	0.702
Toxicity								
Skin sensitization	−	−	−	−	−	−	−	−
Hepatotoxic effect	−	−	−	+	+	+	+	+
Chronic toxic activity (LOAEL)	0.91	1.345	1.025	1.507	0.732	0.132	1.198	1.37
Acute toxic activity (LD$_{50}$)	2.103	2.489	2.281	2.583	2.191	2.627	2.538	2.393
hERG II inhibitor	+	+	−	+	+	+	+	+
hERG I inhibitor	−	−	−	−	−	−	−	−
Max. Tolerated dose	0.116	−0.235	−0.433	0.234	0.557	0.128	0.549	0.839
AMES toxicity	+	+	−	−	+	+	−	−

[a] + = yes while − = No.

according to the results collected (Table 4). As a result, they may exhibit an astonishingly high bioavailability through GIT. Our synthetic compounds can penetrate the central nervous system (CNS) (CNS permeability range: −1.644 to −2.654).

It is generally known that erlotinib, sorafenib, and our derivatives 5, 6, 9, 10 and 14 may inhibit CYP3A4, the main enzyme responsible for drug metabolism. The overall clearance, which is a crucial consideration in choosing dosage intervals, predicted elimination. Compared to sorafenib and our drugs, which had extremely low clearance values, the findings exhibited that erlotinib had superior clearance rates. Erlotinib should thus have shorter dose intervals since it might be eliminated more quickly. In contrast to erlotinib, the synthesized compounds showed a slow clearance rate, which denotes a prolonged half-life and wider dosage windows. The final analyzed factor for the ADMET profile is toxicity. As shown in Table 4, the disadvantage of unintended hepatotoxic effects was shared by sorafenib, erlotinib, and our drugs 9, 10 and 14, but not by 5, 6 and 7. The drug with the greatest maximum tolerated dose was erlotinib. The maximum tolerable dosages for sorafenib and our derivatives, however, were lower. Lastly, the acute toxic doses of our novel compounds are nearly the same as that of sorafenib and erlotinib. Also, the oral chronic toxic dose of compound 9 is higher than that of both sorafenib and erlotinib while that of compound 6 is higher than that of sorafenib and nearly equipotent to that of erlotinib. These data revealed that our derivatives have good therapeutic index.

3 Conclusion

In conclusion, novel isoxazole, pyrazole, triazole, and/or triazine heterocyclic moieties attached to the azobenzene scaffold have been designed, synthesized, and tested on HCT-116, MCF-7, HepG2, and A549 for their anticancer activities targeting both EGFR[T790M] and VEGFR-2 enzymes. The suggested compound's mechanism of interaction with the EGFR[T790M] and VEGFR-2 receptors was examined through molecular design. The information from the biological screening and the results of the docking studies were strongly linked. Compound 14 was the most potent derivative against the four A549, HepG2, MCF-7 and HCT116 cell lines with IC$_{50}$ = 5.15, 6.236.37 and 8.44 μM respectively. It presented slightly lower activities than sorafenib, (IC$_{50}$ = 4.00, 5.05, 5.58 and 4.04 μM respectively), and revealed higher activities than erlotinib (IC$_{50}$ = 7.73, 13.91, 8.20 and 5.49 μM respectively) against the four cell lines. With reverence to the HepG2 cell lines, derivatives 5, 6 and 10 demonstrated very good anticancer effects with IC$_{50}$ = 7.80, 8.17 and 6.81 μM respectively. Assessment of cytotoxicity against HCT-116 cell lines revealed that derivatives 5 and 10 demonstrated very good anticancer effects with IC$_{50}$ = 8.12 and 9.23 μM respectively. Evaluation of cytotoxicity against MCF-7 cell lines showed that derivatives 5, 6 and 10 demonstrated very good anticancer effects with IC$_{50}$ = 6.98, 9.11 and 7.28 μM respectively. When derivatives 5, 6, 7, 10 and 12 were tested for cytotoxicity against A549 cell lines, it was found that they had excellent anticancer effects, with IC$_{50}$ values ranging from 5.88 to 9.25 μM. The

cytotoxicity of the most powerful derivatives 5, 6, 10 and 14, was evaluated against normal VERO cell lines. With IC$_{50}$ values ranging from 42.32 to 55.20 μM, the results showed that the investigated drugs have modest toxicity against VERO normal cells. In addition all compounds were selected to assess their dual VEGFR-2 and EGFR[T790M] inhibitory effects. Among them, compounds 14, 5 and 10 were found to be the most potent that inhibited VEGFR-2 at IC$_{50}$ value of 0.95, 1.25 and 1.50 μM correspondingly. As well, derivatives 14, 6, 5 and 10 could inhibit EGFR[T790M] activity demonstrating strongest effects with IC$_{50}$ = 0.25, 0.35, 0.40 and 0.50 μM respectively. Additionally, the highly active derivatives 5, 6, 10 and 14 in both VEGFR-2 and EGFR[T790M] proteins were subjected to a molecular dynamics (MD) simulation in order to evaluate our molecular modeling findings. Furthermore, the ADMET profiles of the most active compounds 5, 6, 7, 9, 10 and 14 were assessed in comparing to sorafenib and erlotinib as the reference drugs. The data obtained indicated that our derivatives could be beneficial as a future design and optimization template to create more powerful dual VEGFR-2 and EGFR[T790M] inhibitors with stronger anticancer analogues.

4 Experimental

4.1 Chemistry

^{1}H NMR and ^{13}C NMR spectra were recorded on a Bruker 400 and 100 MHZ-NMR respectively, with a spectrophotometer at Microanalytical Center, Ain Shams University.

4.1.1 Ethyl 2-cyano-2-{[4-(phenyldiazenyl)phenyl]diazenyl} acetate (2). 4-Aminoazobenzene (1.79 g, 0.1 mol.) was dissolved in (25 mL) of 50% dilute HCl, and then cooled in water ice bath (0–5 °C). An aqueous solution of NaNO$_2$ (0.68 g, in 4 mL water) was added dropwise while contentious stirring. The obtained diazonium chloride was filtered into sodium acetate solution (4 g in 5 mL water) and ethyl cyanoacetate (1.13 mL, 0.1 mol.) in ethanol (7 mL). The reaction mixture was stirred for 30 min and the formed product was filtered and crystallized from ethanol to afford the targeted compound 2.

Orange crystals from ethanol, m.p. = 250–252 °C; IR (KBr, ν, cm^{-1}) 2225 (C≡N), 1741 (C=O), 1489, 1470 (N=N); ^{1}H-NMR (DMSO-d6) δ: 1.24 (t, 3H, CH$_3$CH$_2$), 1.85 (s, 1H, –N=N–CH), 4.15 (q, 2H, CH$_3$CH$_2$), 7.43–7.84 (m, 9H, Ar-H); ^{13}C-NMR (DMSO-d6) δ: 15.3, 58.9, 98.7, 118.4, 120.2 (2), 122.6 (2), 124.3 (2), 129.8 (2), 130.8, 148.2, 152.8, 166.2, 174.7; anal. calcd for C$_{17}$H$_{15}$N$_5$O$_2$: C, 63.55; H, 4.67; N, 21.81; found: C, 63.66; H, 4.59; N, 21.84.

4.1.2 General procedure for preparation of compounds (3–9). A mixture of compound 2 (3.21 g, 0.1 mol) and each of hydroxylamine hydrochloride (0.69 mL, 0.1 mol), hydrazine hydrate (0.5 mL, 0.1 mol), phenyl hydrazine (1.08 mL, 0.1 mol), 2,4-dinitro phenyl hydrazine (1.98 g, 0.1 mol), semicarbazide hydrochloride (1.11 g, 0.1 mol) and/or thiosemicarbazide (0.91 g, 0.1 mol) in the presence of anhydrous K$_2$CO$_3$ (1.38 g, 0.1 mol) was refluxed for 2–6 h in ethanol/acetic acid (20 mL). After cooling the solid obtained solid was collected by filtration. The residue product was washed with ethanol and recrystallized from the proper solvent to give compounds 3–9.

4.1.2.1   3-Amino-4-{2-[4-(phenyldiazenyl)phenyl]hydrazono}-isoxazol-5(4H)-one (3). Orange crystals from methanol, m.p. >300 °C; IR (KBr, ν, cm^{-1}) 3461, 3346 (NH$_2$), 3190 (NH), 1686 (C=O), 1597, 1545 (C=N), 1417 (N=N); ^{1}H-NMR (DMSO-d$_6$) δ: 7.51–7.93 (m, 9H, Ar-H), 8.60 (s, 2H, NH$_2$, D$_2$O exchangeable), 15.95 (s, 1H, NH, D$_2$O exchangeable); ^{13}C-NMR (DMSO-d$_6$) δ: 111.9, 117.5 (2), 122.9 (2), 124.6 (2), 129.9 (2), 131.9, 145.4, 149.2, 152.6, 160.6 and 170.7; MS (*m/z*): 308 (M$^+$, 29.23%), 271 (37.04%), 196 (100%, base peak), 161 (63.98%), 96 (80.35%), 76 (51.94%); anal. calcd for C$_{15}$H$_{12}$N$_6$O$_2$: C, 58.44; H, 3.90; N, 27.27; found: C, 58.29; H, 3.78; N, 27.33.

4.1.2.2   5-Amino-4-{2-[4-(phenyldiazenyl)phenyl]hydrazono}-2,4-dihydro-3H-pyrazol-3-one (4). Black crystals from methanol, m.p. >300 °C; IR (KBr, ν, cm^{-1}) 3378, 3324 (NH$_2$), 3183 (NH), 1682 (C=O), 1635, 1604 (C=N), 1566 (N=N); ^{1}H-NMR (DMSO-d$_6$) δ: 5.95 (s, 2H, NH$_2$, D$_2$O exchangeable), 7.54–7.97 (m, 9H, Ar-H), 10.62 (s, 1H, NH, D$_2$O exchangeable), 13.05 (s, 1H, NH, D$_2$O exchangeable); ^{13}C-NMR (DMSO-d$_6$) δ: 111.9, 117.2 (2), 122.9 (2), 124.7, 129.9, 131.6 (2), 143.9, 145.4, 149.2, 152.5, 160.6 and 161.3; anal. calcd for C$_{15}$H$_{13}$N$_7$O: C, 58.63; H, 4.23; N, 31.92; found: C, 58.49; H, 4.33; N, 32.04.

4.1.2.3   5-Amino-2-phenyl-4-{2-[4-(phenyldiazenyl)phenyl]hydrazono}-2,4-dihydro-3H-pyrazol-3-one (5). Reddish brown crystals from acetic acid, m.p. >300 °C; IR (KBr, ν, cm^{-1}) 3418 (broad, NH$_2$), 3179 (NH), 1683 (C=O), 1469, 1444 (N=N); ^{1}H-NMR (DMSO-d$_6$) δ: 7.56–7.99 (m, 16H, 14 Ar-H & NH$_2$ (D$_2$O exchangeable)), 12.48 (s, 1H, NH, D$_2$O exchangeable); ^{13}C-NMR (DMSO-d$_6$) δ: 105.9, 106.5, 111.8, 117.1, 117.3 (2), 122.9 (2), 124.7 (2), 129.9 (2), 131.7 (2), 131.8 (2), 144.0, 145.0, 149.1, 152.5, 161.2; MS (*m/z*): 383 (M$^+$, 2.22%), 367 (100%, base peak), 366 (60.07%), 175 (35.79%), 115 (84.99%), 91 (97.54%); anal. calcd for C$_{21}$H$_{17}$N$_7$O: C, 65.80; H, 4.44; N, 25.59; found: C, 65.74; H, 4.35; N, 26.06.

4.1.2.4   5-Amino-2-(2,4-dinitrophenyl)-4-{2-[4-(phenyldiazenyl)phenyl]hydrazono}-2,4-dihydro-3H-pyrazol-3-one (6). Brown crystals from acetic acid, m.p. = 188–190 °C; IR (KBr, ν, cm^{-1}) 3445 (broad, NH$_2$), 3164 (NH), 1685 (C=O), 1469, 1444 (N=N); ^{1}H-NMR (DMSO-d$_6$) δ: 7.55–7.99 (m, 14H, 12 Ar-H & NH$_2$, (D$_2$O exchangeable)), 12.49 (s, 1H, NH, D$_2$O exchangeable); ^{13}C-NMR (DMSO-d$_6$) δ: 105.5, 108.5, 112.1, 117.3 (2), 122.8 (2), 122.9 (2), 124.7 (2), 129.9 (2), 131.6, 138.5, 141.9, 145.8, 149.8, 152.5, 155.3, 161.4; MS (*m/z*): 473 (M$^+$, 1.88%), 386 (23.95%), 162 (35.91%), 103 (100%, base peak), 77 (92.77%); anal. calcd for C$_{21}$H$_{15}$N$_9$O$_5$: C, 53.28; H, 3.17; N, 26.64; found: C, 53.33; H, 3.06; N, 26.70.

4.1.2.5   3-Amino-5-oxo-4-{[4-(phenyldiazenyl)phenyl]diazenyl}-4,5-dihydro-1H-pyrazole-1-carboxamide (7). Brown crystals from methanol, m.p. = 214–216 °C; IR (KBr, ν, cm^{-1}) 3381, 3325 (NH$_2$), 3186 (NH), 1683 (C=O), 1636, 1604 (C=N), 1495 (N=N); ^{1}H-NMR (DMSO-d$_6$) δ: 5.86 (s, 2H, NH$_2$, D$_2$O exchangeable), 7.53–7.94 (m, 11H, 9 Ar-H & NH$_2$ (D$_2$O exchangeable)), 11.59 (s, 1H, NH, D$_2$O exchangeable); ^{13}C-NMR (DMSO-d$_6$) δ: 116.2 (2), 122.9 (2), 124.7 (2), 125.9, 129.9 (2), 131.6, 145.1, 148.7, 150.3, 152.6, 158.8, 160.0; MS (*m/z*): 350 (M$^+$, 15.31%), 301 (100%, base peak), 300 (44.03%), 265 (83.38%), 126 (74.51%); anal. calcd for C$_{16}$H$_{14}$N$_8$O$_2$: C, 54.86; H, 4.00; N, 32.00; found: C, 54.97; H, 3.89; N, 32.12.

4.1.2.6   N-[4-(Phenyldiazenyl)phenyl]-5-thioxo-2,5-dihydro-1H-1,2,4-triazole-3-carbohydrazonoyl-cyanide (9). Orange crystals from acetone, m.p. = 266–268 °C; IR (KBr, ν, cm^{-1}) 3500–2500 (broad, NH), 2226 (C≡N), 1625 (C=N), 1522 (N=N), 1252 (C=S); ^{1}H-NMR (DMSO-d$_6$) δ: 4.49 (s, 1H, NH, D$_2$O exchangeable), 7.19–7.99 (m, 10H, 9 Ar-H & NH (D$_2$O exchangeable)), 8.62 (s, 2H, 2NH, D$_2$O exchangeable); ^{13}C-NMR (DMSO-d$_6$) δ: 105.4, 112.3, 117.4 (2), 122.9 (2), 124.7 (2), 129.9 (2), 131.6, 146.1, 149.0, 152.5, 161.6, 181.6; MS (*m/z*): 348 (M$^+$, 11.00%), 326 (15.09%), 184 (37.37%), 177 (100%, base peak), 169 (48.79%), 65 (65.76%); anal. calcd for C$_{16}$H$_{12}$N$_8$S: C, 55.17; H, 3.45; N, 32.18; S, 9.20; found: C, 55.02; H, 3.54; N, 32.13; S, 9.31.

4.1.3   General procedure for preparation of compounds (10–14). A mixture of compound **2** (3.21 g, 0.1 mol.) and each of phenyl isothiocyanate (1.35 mL, 0.1 mol), thiourea (0.76 g, 0.1 mol), urea (0.6 g, 0.1 mol), guanidine hydrochloride (0.95 g, 0.1 mol), and/or sulphaguanidine (2.14 g, 0.1 mol) was refluxed for 5–12 h in dioxane (10 mL). After cooling the mixture was poured into ice water (100 mL), the formed solid was filtered off, washed with water, recrystallized from the proper solvent to give compounds **10–14**.

4.1.3.1   5-Oxo-4-phenyl-2-[4-(phenyldiazenyl)phenyl]-3-thioxo-2,3,4,5-tetrahydro-1,2,4-triazine-6-carbonitrile (10). Orange crystals from ethanol, m.p. 284–286 °C; IR (KBr, ν, cm^{-1}) 2224 (C≡N), 1683 (C=O), 1596 (C=N); ^{1}H-NMR (DMSO-d$_6$) δ: 7.13–7.99 (m, 14H, Ar-H); ^{13}C-NMR (DMSO-d$_6$) δ: 117.2, 117.3, 122.8, 124.1 (4), 124.7 (2), 124.9, 128.9 (4), 129.2 (2), 129.9, 139.9, 149.1, 152.5, 180.1; anal. calcd for C$_{22}$H$_{14}$N$_6$OS: C, 64.39; H, 3.41; N, 20.49; S, 7.80; found: C, 64.21; H, 3.49; N, 20.61; S, 7.77.

4.1.3.2   5-Oxo-2-[4-(phenyldiazenyl)phenyl]-3-thioxo-2,3,4,5-tetrahydro-1,2,4-triazine-6-carbonitrile (11). Reddish brown crystals from acetone, m.p. >300 °C; IR (KBr, ν, cm^{-1}) 2224 (C≡N), 1680 (C=O), 1622, 1598 (C=N), 1520 (N=N), 1237 (C=S); ^{1}H-NMR (DMSO-d$_6$) δ: 7.56–7.99 (m, 9H, Ar-H), 11.27 (s, 1H, NH, D$_2$O exchangeable); ^{13}C-NMR (DMSO-d$_6$) δ: 105.8, 111.8, 113.9, 116.0, 117.2 (2), 122.9 (2), 124.7 (2), 129.9 (2), 131.8, 149.1, 152.5, 201.5; anal. calcd for C$_{16}$H$_{10}$N$_6$OS: C, 57.49; H, 2.99; N, 25.15; S, 9.58; found: C, 57.55; H, 3.08; N, 25.03; S, 9.44.

4.1.3.3   3,5-Dioxo-2-[4-(phenyldiazenyl)phenyl]-2,3,4,5-tetrahydro-1,2,4-triazine-6-carbonitrile (12). Brown crystals from methanol, m.p. 280–284 °C; IR (KBr, ν, cm^{-1}) 3177 (NH), 2225 (C≡N), 1680 (C=O), 1598 (C=N), 1522 (N=N); ^{1}H-NMR (DMSO-d$_6$) δ: 7.49–8.00 (m, 9H, Ar-H), 12.44 (s, 1H, NH, D$_2$O exchangeable); ^{13}C-NMR (DMSO-d$_6$) δ: 113.9, 116.0, 117.2 (2), 122.9 (2), 124.7 (2), 129.9 (2), 131.7, 143.9, 145.2, 149.1, 152.5, 161.2; anal. calcd for C$_{16}$H$_{10}$N$_6$O$_2$: C, 60.38; H, 3.14; N, 26.42; Found: C, 60.49; H, 3.07; N, 26.55.

4.1.3.4   3-Imino-5-oxo-2-[4-(phenyldiazenyl)phenyl]-2,3,4,5-tetrahydro-1,2,4-triazine-6-carbonitrile (13). Brown crystals from acetic acid, m.p. 276–278 °C; IR (KBr, ν, cm^{-1}) 3174 (NH), 2222 (C≡N), 1679 (C=O), 1597 (C=N), 1520 (N=N); ^{1}H-NMR (DMSO-d$_6$) δ: 7.36–8.06 (m, 9H, Ar-H), 12.64 (s, 2H, 2NH, D$_2$O exchangeable); ^{13}C-NMR (DMSO-d$_6$) δ: 105.7, 111.9, 117.3 (2), 122.9 (2), 124.7 (2), 129.9 (2), 131.7, 144.0, 145.4, 149.1, 152.5, 161.3; MS (*m/z*): 317 (M$^+$, 19.14%), 269 (100%, base peak), 250 (60.16%), 188 (84.71%), 174 (51.62%); anal. calcd for

$C_{16}H_{11}N_7O$: C, 60.57; H, 3.47; N, 30.91; found: C, 60.51; H, 3.33; N, 31.06.

4.1.3.5 4-[(4-Aminophenyl)sulfonyl]-3-imino-5-oxo-2-[4-(phenyldiazenyl)phenyl]-2,3,4,5-tetrahydro-1,2,4-triazine-6-carbonitrile (14). Brown crystals from methanol, m.p. >300 °C; IR (KBr, v, cm^{-1}) 3366, 3329 (broad, NH$_2$), 3215 (NH), 2225 (C≡N), 1681 (C=O), 1621, 1599 (C=N), 1501 (N=N); ^{1}H-NMR (DMSO-d$_6$) δ: 5.67 (s, 2H, NH$_2$, D$_2$O exchangeable), 6.53–7.99 (m, 13H, Ar-H), 9.68 (s, 1H, NH, D$_2$O exchangeable); ^{13}C-NMR (DMSO-d$_6$) δ: 105.9, 106.5, 111.8, 117.1, 117.3 (2), 122.8, 122.9 (2), 124.6, 124.7 (2), 129.9 (2), 131.7, 131.8, 144.0, 145.0, 149.1, 152.5, 160.7, 161.2; MS (m/z): 472 (M$^+$, 7.13%), 451 (20.61%), 340 (24.14%), 312 (32.65%), 266 (100%, base peak); anal. calcd for $C_{22}H_{16}N_8O_3S$: C, 55.93; H, 3.40; N, 23.73; S, 6.78; found: C, 56.06; H, 3.37; N, 23.70; S, 6.89.

4.2 Conventional and microwave methods comparison

In the microwave reactions, the same reactants amounts in the thermal technique were used. The reaction completion was monitored by using TLC. The reaction mixtures were washed with ethanol and crystallized from the suitable solvent. Anton Paar (monowave 300) was used for microwave irradiation reactions using borosilicate glass vials of 10 mL.

4.3 Docking studies

Both VEGFR-2 (PDB ID 4ASD)[51] and EGFR^{T790M} (PDB ID 3W2O)[45] were used by Molsoft program to carry out docking studies (ESI†).

4.4 Molecular dynamics simulation

The highly active derivatives **5**, **6**, **10** and **14** were simulated using molecular dynamics (MD) in VEGFR-2 and EGFR^{T790M} With the help of GAFF2 (ref. 52 and 53) (ESI†).

4.5 Biological testing

4.5.1 In vitro anti-cancer activity. Our derivatives **3–14** was tested against four cell lines, HCT-116, HepG2, MCF-7 and A549 using MTT colorimetric assay[56–58] (ESI†).

4.5.2 In vitro VEGFR-2 assay. All compounds were assessed for their inhibitory activities against VEGFR-2 (ref. 59) (ESI†).

4.5.3 EGFR^{T790M} assay. Using the HTRF assay, all drugs were assessed for their ability to inhibit mutant EGFR^{T790M} (ref. 61) (ESI†).

Conflicts of interest

There is no interest to declare.

Acknowledgements

References

1 R. Reddyrajula, U. Dalimba and S. M. Kumar, Molecular hybridization approach for phenothiazine incorporated 1,2,3-triazole hybrids as promising antimicrobial agents: design, synthesis, molecular docking and *in silico* ADME studies, *Eur. J. Med. Chem.*, 2019, **168**, 263–282, DOI: **10.1016/j.ejmech.2019.02.010**.

2 M. R. C. de Castro, R. F. Naves, A. Bernardes, C. C. da Silva, C. N. Perez, A. F. Moura, M. O. de Moraes and F. T. Martins, Tandem chalcone-sulfonamide hybridization, cyclization and further Claisen–Schmidt condensation: tuning molecular diversity through reaction time and order and catalyst, *Arabian J. Chem.*, 2020, **13**, 1345–1355, DOI: **10.1016/j.arabjc.2017.11.005**.

3 L. M. Moreno, J. Quiroga, R. Abonia, A. Lauria, A. Martorana, H. Insuasty and B. Insuasty, Synthesis, biological evaluation, and *in silico* studies of novel chalcone- and pyrazoline-based 1,3,5-triazines as potential anticancer agents, *RSC Adv.*, 2020, **10**, 34114, DOI: **10.1039/D0RA06799G**.

4 H. E. Hashem, A. E.-G. E. Amr, E. S. Nossier, M. M. Anwar and E. M. Azmy, New Benzimidazole-, 1,2,4-Triazole-, and 1,3,5-Triazine-Based Derivatives as Potential EGFRWT and EGFR^{T790M} Inhibitors: Microwave-Assisted Synthesis, Anticancer Evaluation, and Molecular Docking Study, *ACS Omega*, 2022, **7**(8), 7155–7171, DOI: **10.1021/acsomega.1c06836**.

5 E. T. Warda, I. A. Shehata, M. B. El-Ashmawy and N. S. El-Gohary, New series of isoxazole derivatives targeting EGFR-TK: synthesis, molecular modeling and antitumor evaluation, *Bioorg. Med. Chem.*, 2020, **28**(21), 115674, DOI: **10.1016/j.bmc.2020.115674**.

6 N. M. Saleh, M. G. El-Gazzar, H. M. Aly and R. A. Othman, Novel Anticancer Fused Pyrazole Derivatives as EGFR and VEGFR-2 Dual TK Inhibitors, *Front. Chem.*, 2020, **7**, 917, DOI: **10.3389/fchem.2019.00917**.

7 R. Dahmani, M. Manachou, S. Belaidi, S. Chtita and S. Boughdiri, Structural characterization and QSAR modeling of 1,2,4-triazole derivatives as α-glucosidase inhibitors, *New J. Chem.*, 2021, **45**, 1253–1261, DOI: **10.1039/D0NJ05298A**.

8 A. El-Faham, M. Farooq, Z. Almarhoon, R. Abd Alhameed, M. A. M. Wadaan, B. G. de la Torre and F. Albericio, Di- and trisubstituted s-triazine derivatives: synthesis, characterization, anticancer activity in human breast-cancer cell lines, and developmental toxicity in zebrafish embryos, *Bioorg. Chem.*, 2020, **94**, 103397, DOI: **10.1016/j.bioorg.2019.103397**.

9 B. Zhang, Q. Zhang, Z. Xiao, X. Sun, Z. Yang, Q. Gu, Z. Liu, T. Xie, Q. Jin, P. Zheng, S. Xu and W. Zhu, Design, synthesis and biological evaluation of substituted 2-(thiophen-2-yl)-1,3,5-triazine derivatives as potential dual PI3Kα/mTOR inhibitors, *Bioorg. Chem.*, 2020, **95**, 103525, DOI: **10.1016/j.bioorg.2019.103525**.

10 I. Karakaya, Synthesis and Characterization of Azobenzene Derived from 8-aminoquinoline in Aqueous Media, *J. Turk. Chem. Soc., Sect.*, 2022, **9**(1), 85–114.

11 J. Zhu, T. Guo, Z. Wang and Y. Zhao, Triggered azobenzene-based prodrugs and drug delivery systems, *J. Controlled Release*, 2022, **345**, 475–493, DOI: **10.1016/j.jconrel.2022.03.041**.

12 M. Di Martino, L. Sessa, M. Di Matteo, B. Panunzi, S. Piotto and S. Concilio, Azobenzene as Antimicrobial Molecules, *Molecules*, 2022, **27**, 5643, DOI: **10.3390/molecules27175643**.

13 K. Hüll, J. Morstein and D. Trauner, In vivo photopharmacology, *Chem. Rev.*, 2018, **118**, 10710–10747.

14 O. Leippe and J. A. Frank, Designing azobenzene-based tools for controlling neurotransmission, *Curr. Opin. Struct. Biol.*, 2019, **57**, 23–30.

15 A. E. Berizzi and C. Goudet, Strategies and considerations of G-protein-coupled receptor photopharmacology, *Adv. Pharmacol.*, 2020, **88**, 143–172.

16 P. Wu and D. Manna, Optochemical control of protein degradation, *ChemBioChem*, 2020, **21**, 2250–2252.

17 J. Morstein, A. C. Impastato and D. Trauner, Photoswitchable lipids, *ChemBioChem*, 2021, **22**, 73–83.

18 J. Li, X. Wang and X. Liang, Modification of nucleic acids by azobenzene derivatives and their applications in biotechnology and nanotechnology, *Chem.–Asian J.*, 2014, **9**, 3344–3358.

19 N. M. Saleh, M. S. A. El-Gaby, K. El-Adl and N. E. A. Abd El-Sattar, Design, green synthesis, molecular docking and anticancer evaluations of diazepam bearing sulfonamide moieties as VEGFR-2 inhibitors, *Bioorg. Chem.*, 2020, **104**, 104350, DOI: **10.1016/j.bioorg.2020.104350**.

20 M. L. D. C. Barbosa, L. M. Lima, R. Tesch, C. M. R. SantAnna, F. Totzke, M. H. G. Kubbutat, C. Schachtele, S. A. Laufer and E. J. Barreiro, Novel 2-chloro-4-anilino-quinazoline derivatives as EGFR and VEGFR-2 dual inhibitors, *Eur. J. Med. Chem.*, 2014, **71**, 1–14.

21 A. Garofalo, L. Goossens, A. Lemoine, S. Ravez, P. Six, M. Howsam, A. Farce and P. Depreux, *Med. Chem. Commun.*, 2011, **2**, 65–72, DOI: **10.1039/C0MD00183J**.

22 S. Wilhelm, *et al.*, Discovery and development of sorafenib: a multikinase inhibitor for treating cancer, *Nat. Rev. Drug Discovery*, 2006, **5**(10), 835–844.

23 A. Pircher, *et al.*, Biomarkers in tumor angiogenesis and anti-angiogenic therapy, *Int. J. Mol. Sci.*, 2011, **12**(10), 7077–7099.

24 M. H. El-Shershaby, K. M. El-Gamal, A. H. Bayoumi, K. El-Adl, H. E. A. Ahmed and H. S. Abulkhair, Synthesis, antimicrobial evaluation, DNA gyrase inhibition, and *in silico* pharmacokinetic studies of novel quinoline derivatives, *Arch. Pharm.*, 2020, e2000277, DOI: **10.1002/ardp.202000277**.

25 A. Turky, A. H. Bayoumi, F. F. Sherbiny, K. El-Adl and H. S. Abulkhair, Unravelling the anticancer potency of 1,2,4-triazole-N-arylamide hybrids through inhibition of STAT3: synthesis and *in silico* mechanistic studies, *Mol. Diversity*, 2020, 10131, DOI: **10.1007/s11030-020-10131-0**.

26 M. A. El-Zahabi, H. Sakr, K. El-Adl, M. Zayed, A. S. Abdelraheem, S. I. Eissa, H. Elkady and I. H. Eissa, Design, synthesis, and biological evaluation of new challenging thalidomide analogs as potential anticancer immunomodulatory agents, *Bioorg. Chem.*, 2020, **104**, 104218, DOI: **10.1016/j.bioorg.2020.104218**.

27 K. El-Adl, *et al.*, Design, synthesis, molecular docking and anticancer evaluations of 5-benzylidenethiazolidine-2,4-dione derivatives targeting VEGFR-2 enzyme, *Bioorg.*

Chem., 2020, **102**, 104059, DOI: **10.1016/j.bioorg.2020.104059**.

28 A. G. A. El-Helby, H. Sakr, I. H. Eissa, A. A. Al-Karmalawy and K. El-Adl, Benzoxazole/benzothiazole-derived VEGFR-2 inhibitors: design, synthesis, molecular docking, and anticancer evaluations, *Arch. Pharm.*, 2019, **352**(12), 1900178.

29 K. El-Adl, *et al.*, Design, synthesis, docking, anticancer and *in silico* pharmacokinetic studies of novel 5-([4-chloro/2,4-dichloro]benzylidene)thiazolidine-2,4-dione derived VEGFR-2 inhibitors, *Arch. Pharm.*, 2020, e202000279, DOI: **10.1002/ardp.202000279**.

30 A.-G. A. El-Helby, H. Sakr, R. R. A. Ayyad, K. El-Adl, M. M. Ali and F. Khedr, Design, Synthesis, *In Vitro* Anti-cancer Activity, ADMET Profile and Molecular Docking of Novel Triazolo [3, 4-a] phthalazine Derivatives Targeting VEGFR-2 Enzyme, *Anti-Cancer Agents Med. Chem.*, 2018, **18**(8), 1184–1196.

31 A. G. A. El-Helby, R. R. A. Ayyad, H. Sakr, K. El-Adl, M. M. Ali and F. Khedr, Design, Synthesis, Molecular Docking, and Anticancer Activity of Phthalazine Derivatives as VEGFR-2 Inhibitors, *Arch. Pharm.*, 2017, **350**(12), 1700240.

32 K. El-Adl, M.-K. Ibrahim, F. Khedr, H. S. Abulkhair and I. H. Eissa, *N*-substituted-4-phenylphthalazin-1-amine derived VEGFR-2 inhibitors: design, synthesis, molecular docking, and anticancer evaluation studies, *Arch. Pharm.*, 2020, e2000219, DOI: **10.1002/ardp.2020002190**.

33 K. El-Adl, A. A. El-Helby, R. R. Ayyad, H. A. Mahdy, M. M. Khalifa, H. A. Elnagar, A. B. M. Mehany, A. M. Metwaly, M. A. Elhendawy, M. M. Radwan, M. A. ElSohly and I. H. Eissa, Design,synthesis, and anti-proliferative evaluation of new quinazolin-4(3H)-ones as potential VEGFR-2 inhibitors, *Bioorg. Med. Chem.*, 2021, **29**, 115872, DOI: **10.1016/j.bmc.2020.115872**.

34 N. S. Hanafy, N. A. A. M. Aziz, S. S. A. El-Hddad, M. A. Abdelgawad, M. M. Ghoneim, A. F. Dawood, S. Mohamady, K. El-Adl and S. Ahmed, Design, synthesis, and docking of novel thiazolidine-2,4-dione multitarget scaffold as new approach for cancer treatment, *Arch. Pharm.*, 2023, e2300137, DOI: **10.1002/ardp.202300137**.

35 N. A. A. M. Aziz, R. F. George, K. El-Adl and W. R. Mahmoud, Design, synthesis, and docking of novel thiazolidine-2,4-dione multitarget scaffold as new approach for cancer treatment, *Arch. Pharm.*, 2022, e2200465, DOI: **10.1002/ardp.202200465**.

36 N. E. A. A. El-Sattar, S. E. S. A. El-Hddad, M. M. Ghobashy, A. A. Zaher and K. El-Adl, Nanogel-mediated drug delivery system for anticancer agent: pH stimuli responsive poly(ethylene glycol/acrylic acid) nanogel prepared by gamma irradiation, *Bioorg. Chem.*, 2022, **127**, 105972, DOI: **10.1016/j.bioorg.2022.105972**.

37 H. Elkady, K. El-Adl, H. Sakr, A. S. Abdelraheem, S. I. Eissa and M. A. El-Zahabi, Novel promising benzoxazole/benzothiazole-derived immunomodulatory agents: design, synthesis, anticancer evaluation, and *in silico* ADMET analysis, *Arch. Pharm.*, 2023, **356**(9), e2300097, DOI: **10.1002/ardp.202300097**.

38 D. Adel, K. El-Adl, T. Nasr, T. M. Sakr and W. Zaghary, Pyrazolo[3,4-d]pyrimidine derivatives as EGFR^{T790M} and

VEGFR-2 dual TK inhibitors: design, synthesis, molecular docking, ADMET profile and anticancer evaluations, *J. Mol. Struct.*, 2023, **1291**, 136047, DOI: **10.1016/j.molstruc.2023.136047**.

39 A. M. Sayed, F. A. Taher, M. R. K. Abdel-Samad, M. S. A. El-Gaby, K. El-Adl and N. M. Saleh, Design, synthesis, molecular docking, *in silico* ADMET profile and anticancer evaluations of sulfonamide endowed with hydrazone-coupled derivatives as VEGFR-2 inhibitors, *Bioorg. Chem.*, 2021, **108**, 104669, DOI: **10.1016/j.bioorg.2021.104669**.

40 N. M. Saleh, A. A. Abdel-Rahman, A. M. Omar, M. M. Khalifa and K. El-Adl, Pyridine-derived VEGFR-2 inhibitors: Rational design, synthesis, anticancer evaluations, *in silico* ADMET profile, and molecular docking, *Arch. Pharm.*, 2021, **354**(8), e2100085, DOI: **10.1002/ardp.202100085**.

41 Q.-Q. Xie, *et al.*, Pharmacophore modeling studies of type I and type II kinase inhibitors of Tie2, *J. Mol. Graphics Modell.*, 2009, **27**(6), 751–758.

42 K. Lee, *et al.*, Pharmacophore modeling and virtual screening studies for new VEGFR-2 kinase inhibitors, *Eur. J. Med. Chem.*, 2010, **45**(11), 5420–5427.

43 V. A. Machado, *et al.*, Synthesis, antiangiogenesis evaluation and molecular docking studies of 1-aryl-3-[(thieno [3, 2-b] pyridin-7-ylthio) phenyl] ureas: discovery of a new substitution pattern for type II VEGFR-2 Tyr kinase inhibitors, *Bioorg. Med. Chem.*, 2015, **23**(19), 6497–6509.

44 F. Sangande, E. Julianti and D. H. Tjahjono, Ligand-Based Pharmacophore Modeling, Molecular Docking, and Molecular Dynamic Studies of Dual Tyrosine Kinase Inhibitor of EGFR and VEGFR2, *Int. J. Mol. Sci.*, 2020, **21**(20), 7779, DOI: **10.3390/ijms21207779**.

45 S. A. Elmetwally, K. F. Saied, I. H. Eissa and E. B. Elkaeed, Design, synthesis and anticancer evaluation of thieno[2,3-d]pyrimidine derivatives as dual EGFR/HER2 inhibitors and apoptosis inducers, *Bioorg. Chem.*, 2019, **88**, 102944, DOI: **10.1016/j.bioorg.2019.102944**.

46 B. M. Essa, A. A. Selim, G. H. Sayed and K. E. Anwer, Conventional and microwave-assisted synthesis, anticancer evaluation, 99mTc-coupling and *in vivo* study of some novel pyrazolone derivatives, *Bioorg. Chem.*, 2022, **125**, 105846, DOI: **10.1016/j.bioorg.2022.105846**.

47 N. E. A. Abd El-Sattar, E. H. K. Badawy, E. Z. Elrazaz and N. S. M. Ismail, Discovery of pyrano[2,3-d] pyrimidine-2,4-dione derivatives as novel PARP-1 inhibitors: design, synthesis and antitumor activity, *RSC Adv.*, 2021, **11**(8), 4454–4464, DOI: **10.1039/D0RA10321G**.

48 M. K. A. Regal, E. Rafat and N. E. A. Abd El-Sattar, Synthesis, characterization, and dyeing performance of some azo thienopyridine and thienopyrimidine dyes based on wool and nylon, *J. Heterocycl. Chem.*, 2020, **57**(3), 1173–1182, DOI: **10.1002/jhet.3854**.

49 K. E. Anwer and G. H. Sayed, Conventional and microwave reactions of 1,3-diaryl-5,4-enaminonitrile-pyrazole derivative with expected antimicrobial and anticancer activities, *J. Heterocycl. Chem.*, 2020, **57**(6), 2339–2353, DOI: **10.1002/jhet.3946**.

50 K. E. Anwer, G. H. Sayed and R. M. Ramadan, Synthesis, spectroscopic, DFT calculations, biological activities and molecular docking studies of new isoxazolone, pyrazolone, triazine, triazole and amide derivatives, *J. Mol. Struct.*, 2022, **1256**, 132513, DOI: **10.1016/j.molstruc.2022.132513**.

51 F. Khedr, M.-K. Ibrahim, I. H. Eissa, H. S. Abulkhair and K. El-Adl, Phthalazine-based VEGFR-2 inhibitors: rationale, design, synthesis, *in silico*, ADMET profile, docking, and anticancer evaluations, *Arch. Pharm.*, 2021, e2100201, DOI: **10.1002/ardp.202100201**.

52 B. R. Miller III, T. D. J. McGee, J. M. Swails, N. Homeyer, H. Gohlke and A. E. Roitberg, MMPBSA.py: An efficient program for end-state free energy calculations, *J. Chem. Theory Comput.*, 2012, **8**(9), 3314–3321.

53 J. A. Maier, C. Martinez, K. Kasavajhala, L. Wickstrom, K. E. Hauser and C. Simmerling, ff14SB: improving the accuracy of protein side chain and backbone parameters from ff99SB, *J. Chem. Theory Comput.*, 2015, **11**(8), 3696–3713.

54 J. Wang, R. M. Wolf, J. W. Caldwell, P. A. Kollman and D. A. Case, Development and testing of a general amber force field, *J. Comput. Chem.*, 2004, **25**(9), 1157–1174.

55 S. El-Hddad, M. Sobhy, A. Ayoub and K. El-Adl, *In silico* molecular docking, dynamics simulation and repurposing of some VEGFR-2 inhibitors based on the SARS-CoV-2-main-protease inhibitor N3, *J. Biomol. Struct. Dyn.*, 2022, 1–15, DOI: **10.1080/07391102.2022.2148000**.

56 T. Mosmann, Rapid colorimetric assay for cellular growth and survival: application to proliferation and cytotoxicity assays, *J. Immunol. Methods*, 1983, **65**(1–2), 55–63, DOI: **10.1016/0022-1759(83)90303-4**.

57 F. M. Freimoser, *et al.*, The MTT [3-(4,5-dimethylthiazol-2-yl)-2,5-diphenyltetrazolium bromide] assay is a fast and reliable method for colorimetric determination of fungal cell densities, *Appl. Environ. Microbiol.*, 1999, **65**(8), 3727–3729.

58 K. El-Adl, *et al.*, Design, synthesis, molecular docking, and anticancer evaluations of 1-benzylquinazoline-2,4(1H,3H)-dione bearing different moieties as VEGFR-2 inhibitors, *Arch. Pharm.*, 2020, e2000068, DOI: **10.1002/ardp.202000068**.

59 S. M. Abou-Seri, *et al.*, 1-Piperazinylphthalazines as potential VEGFR-2 inhibitors and anticancer agents: synthesis and *in vitro* biological evaluation, *Eur. J. Med. Chem.*, 2016, **107**, 165–179.

60 C. Deng, J. Xiong, X. Gu, X. Chen, S. Wu, Z. Wang, D. Wang, J. Tu and J. Xie, Novel recombinant immunotoxin of EGFR specific nanobody fused with cucurmosin, construction and antitumor efficiency in vitro, *Oncotarget*, 2017, **8**(24), 38568–38580.

61 N. A. A. M. Aziz, R. F. George, K. El-Adl and W. R. Mahmoud, Exploration of thiazolidine-2,4-diones as tyrosine kinase inhibitors: design, synthesis, ADMET, docking, and antiproliferative evaluations, *Arch. Pharm.*, 2022, e2200465, DOI: **10.1002/ardp.202200465**.

62 D. E. V. Pires, T. L. Blundell and D. B. Ascher, pkCSM: Predicting Small-Molecule Pharmacokinetic and Toxicity Properties Using Graph-Based Signatures, *J. Med. Chem.*,

2015, **58**(9), 4066–4072, DOI: **10.1021/ acs.jmedchem.5b00104**.

63 C. A. Lipinski, F. Lombardo, B. W. Dominy and P. J. Feeney, Experimental and computational approaches to estimate solubility and permeability in drug discovery and development settings, *Adv. Drug Delivery Rev.*, 1997, **23**(1– 3), 3–25, DOI: **10.1016/S0169-409X(96)00423-1**.

64 A. Beig, R. Agbaria and A. Dahan, Oral Delivery of Lipophilic Drugs: The Tradeoff between Solubility Increase and Permeability Decrease When Using Cyclodextrin-Based Formulation, *PLoS One*, 2013, **8**(10), e68237, DOI: **10.1371/ journal.pone.0068237**.